


Gao Hongchen Jacey Numerical Simulation of RC Slabs Strengthened with Pre-stressed CFRP Laminates

Portugal | 2016


ADVANCED MASTERS IN STRUCTURAL ANALYSIS
OF MONUMENTS AND HISTORICAL CONSTRUCTIONS

Master's Thesis

Gao Hongchen Jacey

Numerical Simulation of RC Slabs Strengthened with Pre-stressed CFRP Laminates

University of Minho

Czech university of Prague

Education and Culture

Erasmus Mundus

ADVANCED MASTERS IN STRUCTURAL ANALYSIS
OF MONUMENTS AND HISTORICAL CONSTRUCTIONS

Master's Thesis

Gao Hongchen Jacey

Numerical Simulation of RC Slabs Strengthened with Pre-stressed CFRP Laminates

This Masters Course has been funded with support from the European Commission. This publication reflects the views only of the author, and the Commission cannot be held responsible for any use which may be made of the information contained therein.

Portugal | 2016

DECLARATION

Name: Gao Hongchen Jacey

Email: jacey.ghc@gmail.com

Title of the Msc Dissertation: Numerical Simulation of RC Slabs Strengthened with Pre-stressed CFRP Laminates

Supervisor(s): Professor Jose Sena-Cruz

Year: 2016

I hereby declare that all information in this document has been obtained and presented in accordance with academic rules and ethical conduct. I also declare that, as required by these rules and conduct, I have fully cited and referenced all material and results that are not original to this work.

I hereby declare that the MSc Consortium responsible for the Advanced Masters in Structural Analysis of Monuments and Historical Constructions is allowed to store and make available electronically the present MSc Dissertation.

University: University of Minho

Date: 18 July 2016

Signature: _____

This page is purposely left blank.

ACKNOWLEDGEMENTS

Firstly, I would like to express my greatest appreciation to the Erasmus Mundus Scholarship sponsored by the European Commission. The learning opportunities and cultural immersion offered by the Erasmus Mundus program is deeply cherished. During the 1 year intensive advanced master program, the vibrant and unique learning experiences in Prague Czech Republic, Guimaraes Portugal as well as Barcelona Spain, are definitely among the most precious memories in life.

I would like to express my gratitude to Professor Jose Sena-Cruz for his supervision and guidance during the course of this dissertation. Moreover, I would like to extend my gratitude to Professor Miguel Azenha for his assistance and advice for numerical modelling. I deeply appreciate their support, suggestions and interesting discussions which contribute to my understanding of the topic. In addition, this study was developed under the auspices of the FRPLongDur R&P project(POCI-01-0145-FEDER-016900 / FCT PTDC/ECM/112396/2009) supported by FEDER funds through the POCI Operational Program, the Operational Program of Lisbon, and National Funds through FCT – Portuguese Foundation for Science and Technology. The contribution of the experimental work is also acknowledged.

Last but not least, my heartfelt appreciation is dedicated to my family, especially my mother, for her unconditional love and continuous encouragement. I am deeply grateful for her unfailing support when making big decisions in life.

This page is purposely left blank.

ABSTRACT

In the recent few decades, carbon fiber reinforced polymer materials (CFRP) have emerged as a common strengthening material for concrete structures due to its advantages such as high strength and stiffness, lightweight, and corrosion resistant. In addition, CFRP exhibits excellent fatigue resistance, low creep deformation and low relaxation. One of the most common strengthening techniques is to apply CFRP as externally bonded reinforcement (EBR). In this technique, the CFRP laminates are externally bonded to the concrete element usually by epoxy adhesives to enhance the flexural strength and stiffness. However, one major limitation of this technique is inefficient mobilization of the high tensile strength of CFRP due to premature debonding. An innovative improvement to overcome the drawbacks is to apply prestress to the CFRP laminates in EBR technique for strengthening reinforced concrete (RC) structures. As a result, the benefits of passive EBR systems are combined with the advantages associated with external prestressing, thus ensuring greater efficiency for flexural strengthening. This dissertation aims to better understand the efficiency of prestressed CFRP laminates for flexural strengthening and to predict different possible failure modes that can occur by using finite element modelling studies.

A nonlinear FEM study on RC slabs strengthened with prestressed CFRP laminates has been carried out using the software DIANA®. Prior to the present study, a total of three slabs, being (i) unstrengthened reference slab; (ii) slab strengthened with un-stressed CFRP by EBR; and (iii) slab strengthened with prestressed CFRP by mechanical anchorage (MA), were tested up to failure under a four-point loading configuration. In addition to this, other slabs were also subjected to sustained loads to assess the long-term structural behavior. All the experimental work was carried out in the scope of the research project FRPreDur (FCOMP-01-0124-FEDER-028865). Detailed FEM studies for each slab have been developed to correlate with the experimental results. Good agreement has been obtained between the experimental and numerical results. The results highlight the improved performance of the CFRP strengthened slabs (both un-stressed and prestressed) in terms of lower deflection, crack width delay and lower crack spacing. In particular, the MA system prevented a premature failure by debonding and allowed the slabs to support higher ultimate loads and deflections. A greater use of the CFRP laminate strip tensile capacity was attained with prestressing.

Based on the existing model, a series of parametric studies have been carried out to investigate the effects of variation of (i) prestress level; (ii) concrete grade; and (iii) CFRP laminate geometry, on the flexural behavior of the strengthened slab. An increase in prestress level provides significant enhancement of load capacity at crack initiation and yielding, and a significant reduction in mid-span deflection at ultimate failure. The variation of concrete grade results minimal enhancement in terms of load capacity and mid-span deflection. By increasing the cross-sectional area of CFRP laminate, the load capacity at crack initiation and yielding is significantly increased, and such enhancement becomes considerably remarkable at ultimate failure.

Finally, an exploratory study on modeling of the creep behavior of RC slabs strengthened with pre-stressed CFRP laminates has been developed. The results seem to be promising, yielding to the conclusion that the existing numerical tools can simulate with enough accuracy the strengthening technique studied.

RESUMO

Nas últimas décadas, o uso de polímeros reforçados com fibras (CFRP - *Carbon Fiber Reinforced Polymer*) têm emergido como material de reforço em estruturas de betão existentes, devido às suas vantagens tais como elevada rigidez e resistência, leveza e resistência à corrosão. Além disso, os CFRP apresentam excelente resistência à fadiga, baixa deformação por fluência e de baixa relaxação. Uma das técnicas de reforço mais comumente usadas recorre à aplicação do reforço (CFRP) nas faces externas dos elementos a reforçar. Esta técnica designa-se por EBR (*Externally Bonded Reinforcement*). Nesta técnica, geralmente, os laminados de CFRP estão fixos externamente ao elemento de betão por intermédio de adesivos de origem epoxídica para melhorar a sua resistência e rigidez à flexão. No entanto, uma das grandes limitações desta técnica está associada à deficiente mobilização da resistência à tração de CFRP devido ao descolamento prematuro deste em relação ao substrato. Melhores resultados podem ser alcançados com recurso à aplicação de pré-esforço aos laminados de CFRP. Como resultado, as vantagens da técnica EBR (passiva) são combinadas com as vantagens associadas ao uso de pré-esforço externo, garantindo assim uma maior eficiência no reforço à flexão. Esta dissertação tem como objetivo compreender melhor a eficiência de laminados de CFRP pré-esforçados no reforço à flexão e prever diferentes modos de rotura possíveis que podem ocorrer através de estudos numéricos com recurso à simulação por intermédio do método dos elementos finitos (FEM).

Foram efetuadas análises numéricas não lineares baseadas no FEM em lajes de betão armado reforçadas com laminados de CFRP pré-esforçado com recurso ao *software* DIANA®. Previamente ao presente estudo, foram experimentalmente ensaiadas três lajes à flexão: (i) uma laje não reforçada (considerada laje de referência); (ii) uma laje reforçada com um laminado de CFRP segundo a técnica EBR; e (iii) uma laje reforçada com um laminado de CFRP pré-esforçado segundo a técnica EBR e recorrendo a chapas de ancoragem nas extremidades (MA – *Mechanical anchorage*). Adicionalmente, lajes foram também submetidos a cargas gravíticas de modo a avaliar-se o comportamento estrutural de longo prazo. Todo o trabalho experimental foi realizado no âmbito do projeto de investigação FRPreDur (FCOMP-01-0124-FEDER-028865). Estudos baseados no FEM de cada laje foram desenvolvidos para as lajes ensaiadas experimentalmente. Uma boa concordância foi obtida entre os resultados experimentais e os modelos numéricos. Os resultados relevam a melhoria do uso CFRP (tanto aplicado de forma

passiva como ativa) em termos de menores deformações, atraso no início da fissuração e propagação da fissuração. Em particular, o sistema MA impediu a rotura prematura por destacamento, e permitiu que as lajes pudessem suportar cargas mais elevadas. Adicionalmente, o pré-esforço permitiu que fossem que fossem atingidas extensões mais elevadas no CFRP.

Com base nos modelos numéricos calibrados, foram realizados estudos paramétricos para investigar os efeitos da variação (i) do nível de pré-esforço; (ii) da resistência à compressão do betão; e (iii) da geometria do laminado de CFRP. Um aumento do nível de pré-esforço proporciona melhoria significativa na carga de início da fissuração e de cedência da armadura longitudinal, e uma redução significativa da flecha a meio do vão na rotura. A variação da resistência do betão conduz a melhorias residuais na capacidade de carga e flecha a meio vão na rotura. Ao aumentar a área da secção transversal do laminado de CFRP, a carga associada ao início de fissuração e cedência das armaduras longitudinais aumentam de forma significativa, e este aumento torna se consideravelmente notável na rotura.

Finalmente, foi desenvolvido um estudo exploratório relativo à simulação numérica do comportamento das lajes reforçadas com laminados de CFRP pré-esforçados devido ao efeito da fluência. Os resultados aparentam serem promissores, levando à conclusão que as ferramentas numéricas existentes pode simular com rigor suficiente as técnicas de reforço estudadas.

Table of Contents

List of Figures

List of Tables

This page is purposely left blank.

CHAPTER 1 INTRODUCTION

1.1 Carbon Fiber Reinforced Polymers (CFRP)

In the recent few decades, fiber reinforced polymer materials (FRP) have emerged as a common strengthening material for concrete structures. FRP is a composite material in the form of unidirectional or multi-directional strips consisting of two different components: the fibers and the polymer matrix (Figure 1.1). Carbon (C) and glass (G) are the main types of fibers composing the fibrous phase of these materials (CFRP and GFRP), whereas epoxy adhesive is generally used in the matrix phase. The fiber is responsible for carrying the load and has high strength. The matrix has the following main objectives: (i) to keep the fibers together; (ii) to protect the fibers against the external actions; (iii) to assure the stress transfer between fibers; and (iv) in some cases, to serve as a bonding material between the FRP and the component to be strengthened. The matrix has relatively low strength and transfer load and stress between fibers [Correia, 2013]. FRP composites are increasingly being considered as an enhancement to or substitute for civil construction materials, namely concrete and steel. FRP composites are lightweight, non-corrosive, exhibit high specific strength and specific stiffness. They are easily constructed and can be tailored to satisfy performance requirements. Due to these advantageous characteristics, FRP composites have been extensively applied in new construction and rehabilitation of structures through its use as reinforcement in concrete, bridge decks, and external reinforcement for strengthening and seismic upgrade [Martin, 2013].

Carbon Fiber Reinforced Polymer composite (CFRP) which contains carbon fibers in the fibrous phase, has been widely used in construction industry due to the advantages mentioned above. Additionally, CFRP presents excellent fatigue resistance, low creep deformation and low relaxation. CFRP for strengthening purpose are commercially available in two main typologies: laminates and sheets, with different properties depending on the application (Figure 1.2). The CFRP laminates have unidirectional precured carbon fibers strips bonded by epoxy matrix while the CFRP sheets have unidirectional or multi-directional mats of continuous carbon fibers impregnated or bonded with epoxy matrix [Correia, 2013]. Its ability to increase the flexural, shear or compressive strength of structural concrete members has been studied and reported in many published literatures, such as Sena-Cruz, 2004; Corrales,

2005; Michels et al., 2013; Correia et al., 2015. CFRP has been extensively used in flexural and shear strengthening of beams and slabs, and column confinement strengthening.

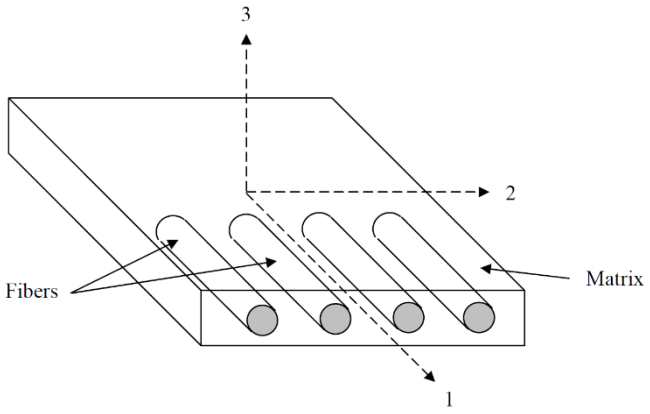

Figure 1.1 Composition of unidirectional FRP-fibers and matrix

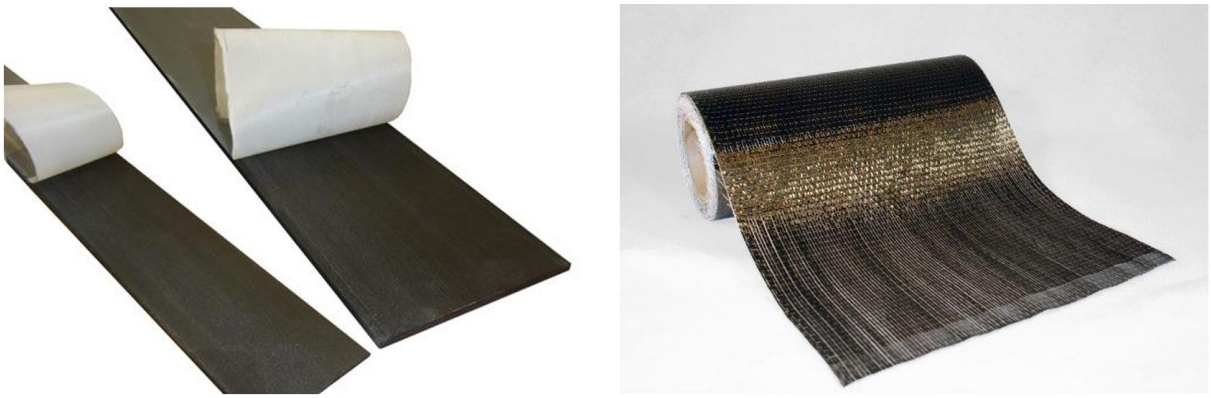

Figure 1.2 CFRP laminates (left) and CFRP sheets (right)

1.2 CFRP used as Externally Bonded Reinforcement

CFRP has been used in different configurations and techniques to deploy the material effectively and to ensure long service life of the selected system. One of the most common strengthening techniques is to apply CFRP as externally bonded reinforcement (EBR). In this technique, the CFRP laminates are externally bonded to the concrete element usually by epoxy adhesives to enhance the flexural strength and stiffness. However, the mounting of an unstressed outer reinforcement (EBR) has the disadvantage of providing a very limited additional stiffness to the structure under service loads. Several publications revealed that this

technique is unable to fully mobilize the tensile strength of CFRP material due to premature debonding [Nguyen et al., 2001; Motavalli et al. 2011; Bilotta et al., 2015]. In most cases, only 20–30 % of the material's capacity is effectively used [Motavalli et al., 2011], and hence, the high tensile strength of CFRP is not fully exploited. Moreover, the reinforcing performance of CFRP materials decreases significantly when exposed to extreme temperature variations [Pantuso et al., 2000]. In addition, since the CFRP materials used in EBR technique are exposed to the environment, they are susceptible to damage caused by vandalism and mechanical malfunctions.

In order to overcome these drawbacks, several improvements have been made with regards to the EBR technique. Near-surface mounted (NSM) is an emerging strengthening technique based on bonding CFRP bars or laminate strips into pre-cut grooves on the concrete. Baschko and Zilch [1999] first published positive experimental results about the use of near-surface mounted CFRP laminate strips as a strengthening technique. As compared to EBR system, NSM is more efficient for strengthening existing reinforced concrete (RC) structures since the debonding phenomenon is less relevant and thus the tensile strength of CFRP materials can be greater exploited [Barros et al., 2006; Bilotta et al., 2015]. Another great innovation for strengthening RC structures is to apply prestress to the CFRP laminates in EBR and NSM systems. The prestressed CFRP for strengthening combines the benefits of passive EBR systems with the advantages associated with external prestressing [Michels et al., 2013]. Recent research by Correria et al. [2015] compared the effect of prestressed CFRP laminate strips for flexural strengthening of RC slabs using different anchorage systems, and revealed that the prestressed CFRP systems are generally more efficient for flexural strengthening than unstressed EBR CFRP laminate strips.

Although there have been several researches showing positive findings about the application of prestressed CFRP laminates as EBR strengthening for RC structures, it should be also noted that CFRP is brittle in nature. It is elastic until it reaches certain strain and suddenly fails without warning. Moreover, the behavior of the interface which bonds CFRP and the strengthening material is difficult to predict. In order to better understand the efficiency of prestressed CFRP laminates for flexural strengthening and to predict different possible failure modes that can occur during the experimental phase, finite element modeling (FEM) studies have been adopted to better envisage the viscoelastic effects experimentally observed.

1.3 Objective and Scope

The R&D FRPreDur Project (FCT reference - PTDC/ECM-EST/2424/2012), developed by the University of Minho and EMPA (Swiss Federal Laboratories for Materials Science and Technology), aiming to assess the short and long-term structural behaviour of concrete elements strengthened in flexure with prestressed CFRP laminates by mechanical anchorage method. To study the viscoelastic effects, reinforced concrete slabs were subjected to sustained loads, being the deformation monitored during a certain period of time. At the end of the long-term structural behaviour assessment, the slabs were then unloaded and monotonically tested up to failure [Sena-Cruz, 2015]. Further information about these tests are elaborated in the following chapters. In order to better understand the results experimentally obtained from the tests up to failure, as well as the viscoelastic effects experimentally observed, numerical simulations must be developed.

Consequently, the main objectives of this dissertation are as follows:

(i) To simulate numerically the experimental results of the prestressed slabs tested up to the failure;
(ii) To simulate numerically the results of the slabs submitted to sustained loads (creep behaviour);
(iii) To perform parametric studies to analyse the effect of relevant variables, such as prestressing level, concrete grade and CFRP laminate geometry.

The FEM numerical simulations will be performed in a software-DIANA TNO version 9.6, for the structural analysis by using models based of fracture mechanics. **DIANA** (**DI**splacement **ANA**lyzer) is an extensive multi-purpose finite element software package that is dedicated to a wide range of structural civil engineering problems. The finite element models in this study are two dimensional, assuming plane stress state.

The scope of this dissertation is specified as follows:

(a) The comparison between numerical and experimental results are mainly in the following aspects: (i) total applied load *versus* displacement at the mid-span for the slabs; (ii) total applied load *versus* top concrete strain (in compression) at mid-span; (iii) total applied

load *versus* CFRP strains at mid-span; (iv) crack patterns; and (v) the total applied load *versus* bottom longitudinal steel strains at mid-span for all slabs are presented and analysed.

(b) Creep test simulation for slab strengthened with prestressed CFRP laminate by MA, including mid-span deflection and relaxation and viscoelastic effects will be addressed.

(c) The parametric studies involves the following variables: (i) prestressing level at 4%, 6% and 8%; (ii) concrete grade of C30/37, C35/45 and C40/50; and (iii) CFRP laminate geometry of L50 × 1.2, L80 × 1.2 and L100 ×1.2. Relevant aspects like cracking, yielding initiation, load carrying capacity and mid-span deflection will be discussed.

1.4 Outline of the Thesis

Chapter 2 presents literature reviews about prestress techniques for EBR CFRP laminate systems. In addition, previous research on the constitutive material models of CFRP strengthened RC structures in finite element analysis will be presented. A brief summary of research significance of this dissertation will be given at the end of the chapter.

Chapter 3 presents a resume of the R&D Project FRPreDur, with emphasis on the experimental tests with slabs. Important results such as deflection of the slabs, influence of prestress level, and crack patterns observed during experiments will be analyzed. A summary of conclusions which can be drawn from the experimental analysis will be given at the end of this chapter.

Chapter 4 presents the finite element models developed to simulate the behavior of the three RC slabs. The selection of constitutive material models for each constituent material, namely, concrete, steel reinforcement, CFRP and the interface, are elaborated in details. The properties of these constituent materials are based on the material characterization performed in the scope of the project. The critical software commands for analysis execution are also presented.

Chapter 5 presents the results and analysis generated from the finite element modelling. Comparisons of numerical and experimental results are made mainly in the following aspects: (i) load *vesus* mid-span displacement; (ii) load *vesus* mid-span concrete strains; (iii) load *vesus* mid-span CFRP strains; (iv) load *vesus* mid-span steel strains; and (v) crack patterns. In

addition, numerical simulation results for creep test is also compared with the experimental results and analysed.

Chapter 6 presents parametric studies based on the models developed and described in the previous chapter. The effects of relevant variables are analyzed, such as (i) prestress level; (ii) concrete grade; and (iii) CFRP laminate geometry. The corresponding numerical results are presented and analyzed.

Chapter 7 summarizes the conclusions from this study. Some recommendations and future work are also suggested.

CHAPTER 2 LITERATURE REVIEWS

2.1 Prestressing Techniques for EBR-CFRP Laminate Systems

2.1.1 Advantages of Prestressing

The Externally Bonded Reinforcement (EBR) technique is the most widely used strategy in the context of reinforced concrete strengthening. As mentioned in Chapter 1, by prestressing the CFRP materials attached to the concrete substrate, the advantages of external prestressing and of the EBR technique are combined and mainly shown in the following aspects [El-Hacha et al., 2001; Michels et al., 2013]: (i) deflection reduction and acting against dead loads; (ii) crack widths reduction; (iii) delay in the onset of cracking; (iv) strain relief within the internal steel reinforcement; (v) higher fatigue failure resistance; (vi) delay in yielding of the internal steel reinforcements; (vii) more efficient use of concrete and FRP; (viii) reduction of premature debonding failure; (ix) increase in ultimate load-bearing capacity; (x) increase in shear capacity. Figure 2.1 illustrates a schematic representation of the moment-curvature (M-χ) relationship for the three situations, namely the unstrengthened reinforced concrete (RC) element, a strengthened RC element with unstressed CFRP laminates (EBR) and a strengthened RC element with prestressed CFRP laminate [Michels et al., 2016]. An enhanced crack, yield, and ultimate load is shown in terms of an increase in the respective bearing moments ΔM_{cr}, ΔM_y and ΔM_u.

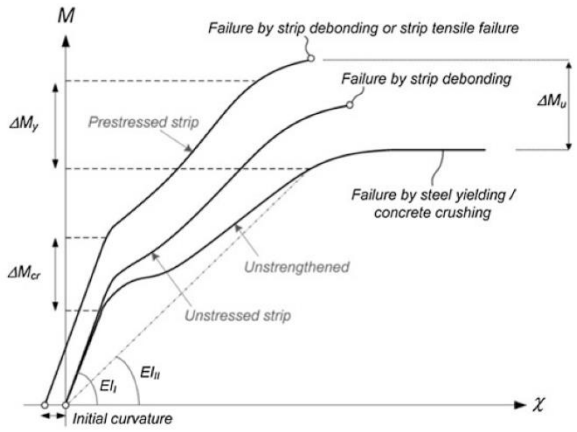

Figure 2.1 Schematic Moment-Curvature relationships for an unstrengthened RC element, a strengthened RC element with an unstressed laminate and a strengthened RC element with a prestressed laminate [Michels et al., 2016]

2.1.2 Types of Prestressing

The available methods of prestressing are reviewed and summarized by El-Hacha et al. [2001]. Generally, there are three methods of prestressing for an existing structure as illustrated in Figure 2.2. The first technique is known as the *cambered beam system*, which requires an initial counter-deflection against the dead-loads by means of hydraulic jacks. Afterwards, the FRP strip is applied and the structure is thus prestressed due to subsequent releasing of the initially inflicted deflection. The second method is the use of an *external support construction*, in which the equipment for prestressing application is being supported against. The third is the *prestressing against the structure* itself. This method requires the previous installation of supporting elements, such as anchor bolts that are used to fix a hydraulic jack. In most cases, these temporary elements are removed after the completion of the retrofitting action. This method is the most common prestressing technique available in the market. Usually, mechanical anchors are used at the strip ends.

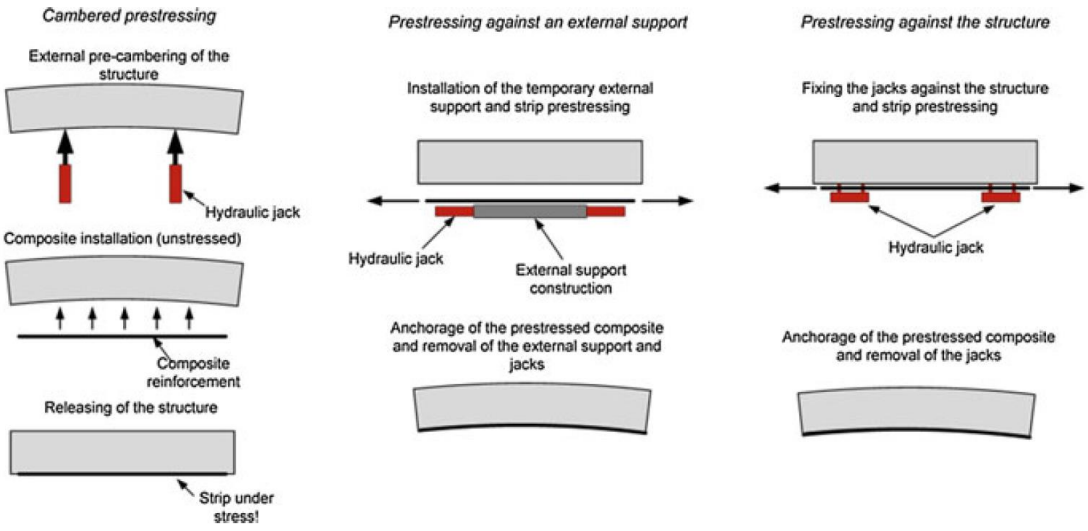

Figure 2.2 Different types of prestressing of an existing RC element [El-Hacha et al., 2001]

2.1.3 Anchorage Systems

It has been recognized that the efficiency of this prestressing technique is directly depend on the type of anchorage used. Schmidt et al. [2012] reviewed a few anchorage systems and reported that compared to a bonded anchorage which requires the instant curing of bonding

agents and needs longer anchorage lengths, a mechanical anchorage is preferred because it is easy to mount and control the stress through it. Correia et al. [2015] investigated the flexural behavior of RC slabs strengthened with CFRP strips using two different anchorage systems, namely mechanical anchorage (MA) and gradient anchorage (GA). For a MA system, the anchors are fixed to concrete substrate while for a GA system, an accelerated epoxy resin curing is necessary, followed by a segment-wise prestress force decrease at the strip ends. The main procedures for prestressing according to MA and GA systems are illustrated in Figure 2.3.

It was reported that both non-prestressed and prestressed EBR strengthening improved the slabs performance with lower deflection, crack width delay and lower crack spacing. Such conclusions were also supported by Sena-Cruz et al. [2015] that the CFRP laminate strip is better exploited when prestressing is used, with slightly higher overall load carrying capacities for MA than for the GA. In particular, the metallic anchors in the MA system prevented a premature debonding failure and thus allowed the slabs to support higher ultimate loads and deflections [Correia et al., 2015]. Sudden strip debonding was observed for GA system, and this phenomenon was similar to conventional EBR without end-fixation. On the other hand, MA system experienced progressive strip debonding which allow to precisely capture the ultimate loading forces [Sena-Cruz, 2015].

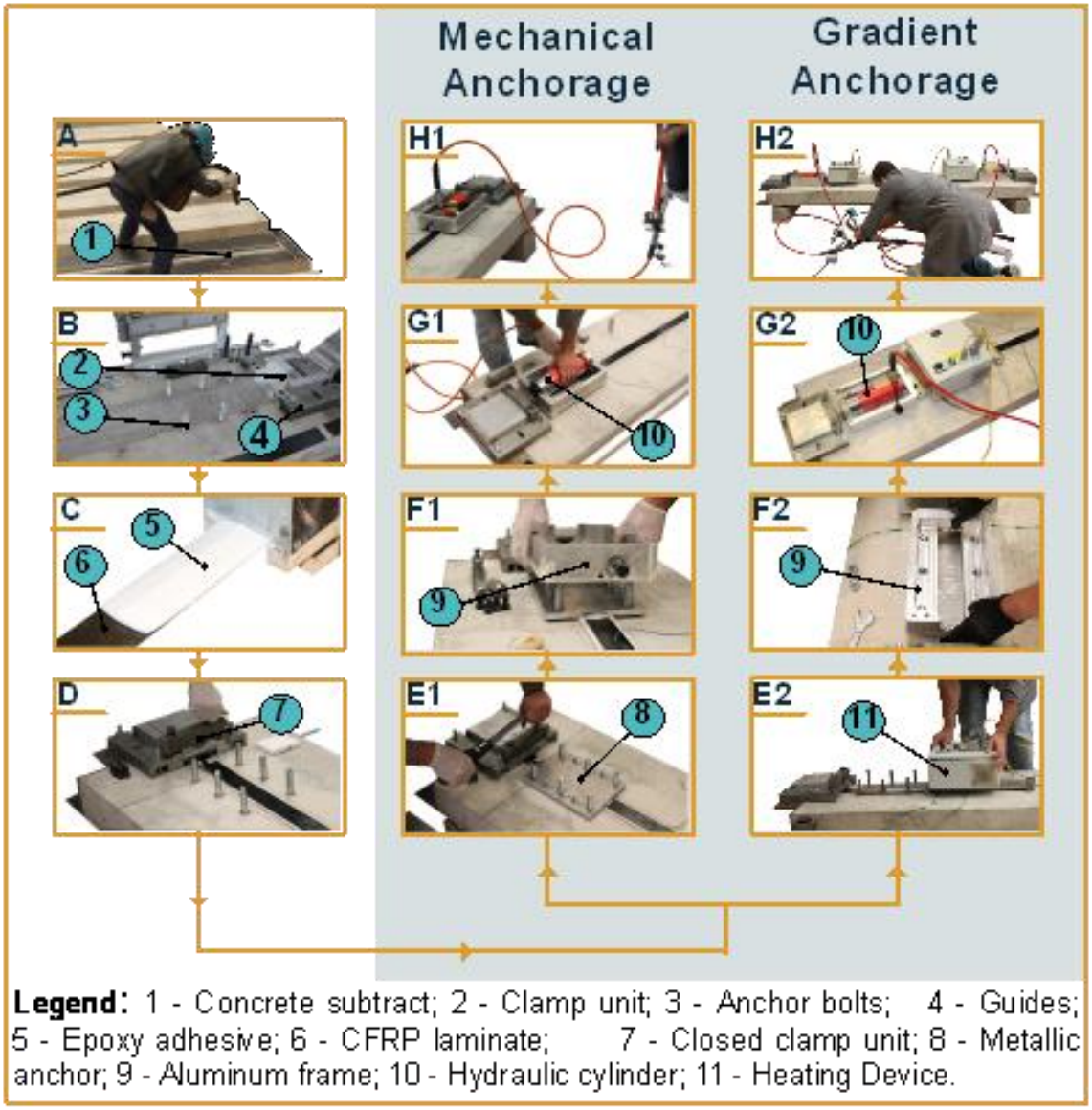

Figure 2.3 Main procedures for prestressing according to MA and GA systems [extracted from Michels et al., 2015]

2.2 Finite Element Modeling

In the recent few decades, finite element models have increasingly gained popularity in structural analysis due to its ability to simulate structural behavior of any structures under various loading conditions. Although a three-dimensional (3D) model is more realistic in most cases, a two-dimensional (2D) model is often chosen which involves less computational effort and time. Despite the limitation that a 2D model does not consider the Poisson's ratio in the out-of-plane direction, there are several publications accurately simulate the behavior of

concrete strengthened with CFRP. The relevant works related to this dissertation are summarized in the following subsections.

2.2.1 Reinforced Concrete Model

To achieve an accurate finite element modelling, it is very critical to adopt the appropriate constitutive material models. Chin et al. [2012] performed a 2D nonlinear finite element analysis of RC beams with large openings in shear strengthened with CFRP laminates using ATENA software, and obtained good correlations between experimental and numerical results. A rotated smeared crack model was adopted. The equivalent uniaxial law which covers the complete range of plane stress behaviour in tension and compression was used to derive the elastic constants as shown in Figure 2.4. The maximum tensile strength is reached linearly, followed by a nonlinear descending softening law, where a fictitious crack model based on crack-opening law and fracture energy was used, implying that cracks occur when the principal stress exceed the tensile strength. The recommendations by CEB-FIP Model Code [1990] has been adopted to assessing the stress-strain relationship of concrete in compression.

In another research work done by Sena-Cruz [2004], a multi-fixed smeared crack model was adopted for non-linear behavior of concrete strengthened with CFRP using FEMIX software. A tri-linear stress-strain diagram, represented in Figure 2.5, is used to simulate the post-cracking behavior of reinforced concrete element. According to the author, the main advantage of this approach is the possibility of changing the values of ξ_1, α_1, ξ_2 and α_2, thus providing enough flexibility in order to model the most important aspects of the tension-stiffening effect.

Corrales [2005] adopted a total strain rotating crack model, which describe the tensile and compressive behavior of concrete with one stress-strain relationship, to simulate the RC beams strengthened with CFRP using lateral anchorage strips. It was also concluded that total strain rotating crack model yielded more accurate representation of concrete behavior than the smeared crack model. The shear behavior of the concrete after cracking is defined as constant shear retention for this model, implying that there is no reduction for shear modulus since the direction of cracks is always perpendicular to the principal stresses. The tensile behavior of concrete was modelled based on Figure 2.6 shown, with mainly two zones: elastic zone which

is linearly ascending and softening zone which is nonlinear following the Hordijk et al. [1991] formulation.

Due to the complexity of non-linearity of concrete, there has been several different material models adopted for different studies on CFRP strengthened RC beams. According to these publications, each model is in good agreement with the respective experimental results. The initial selection of material properties may involve several trials to accurately determine the relevant parameters.

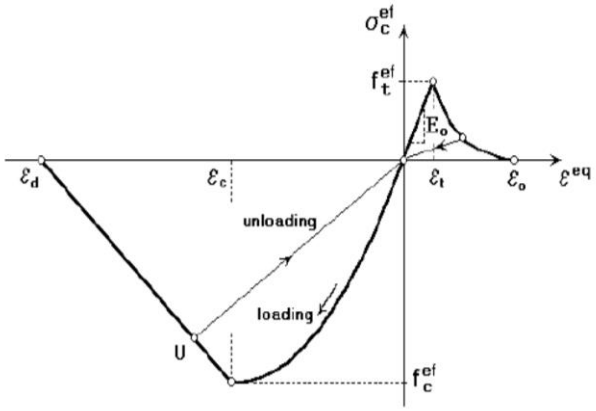

Figure 2.4 Uniaxial stress-strain for concrete [Chin et al., 2012]

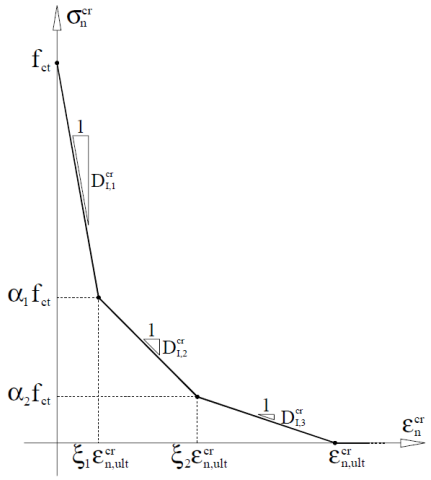

Figure 2.5 Tri-linear tensile softening diagram [Sena-Cruz, 2004]

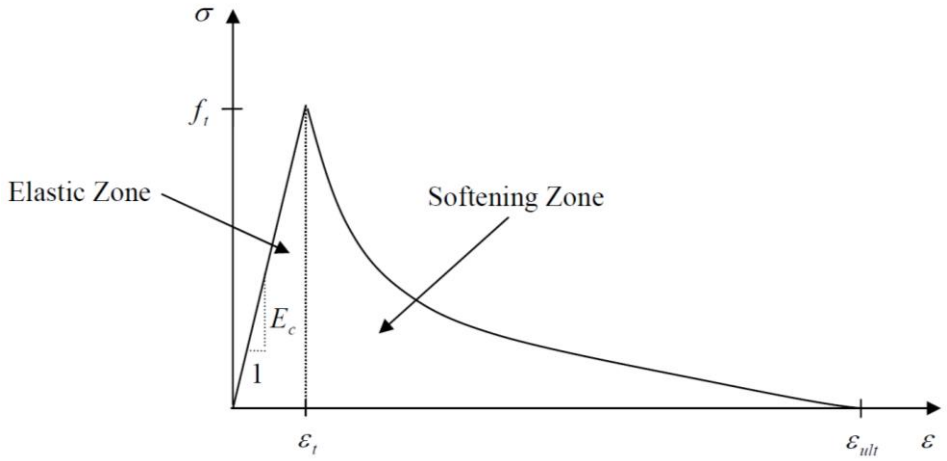

Figure 2.6 Tensile stress-strain behavior of concrete [Correlas, 2005]

2.2.2 Steel Reinforcement

For the case of steel reinforcement, on the other hand, it is relatively easier and straightforward. Sena-Cruz [2004] adopted a uniaxial constitutive model for steel reinforcements as shown in Figure 2.7 which is an idealized stress-strain relationship obtained from standard tensile tests. The curve is defined by three points (PT1, PT2 and PT3 in the figure), composed of four stages: linear elastic stage, yielding plateau, hardening and fracture. Chin et al. [2012] adopted a similar multi-linear stress strain law (as shown in Figure 2.8) which consists of four linear lines, defining the same four stages previously mentioned in the earlier sentence. There is another simplified multi-linear stress strain relationship which consists of two elastic zones: one defined by the yielding stress of the steel f_y and its Young's modulus E_s, and a second one, also called hardening portion, defined by the ultimate f_u and the yielding stress of the steel [Corrales, 2005]. In many cases, bilinear stress strain relationship (Figure 2.9) has been adopted by several researchers for steel reinforcement model [Sena-Cruz et al., 2011]. In such case, the yield stress and ultimate stress as well as their corresponding strains are the necessary parameters to determine the relationship. Perfect bond between steel reinforcements and concrete is often assumed in the numerical simulation.

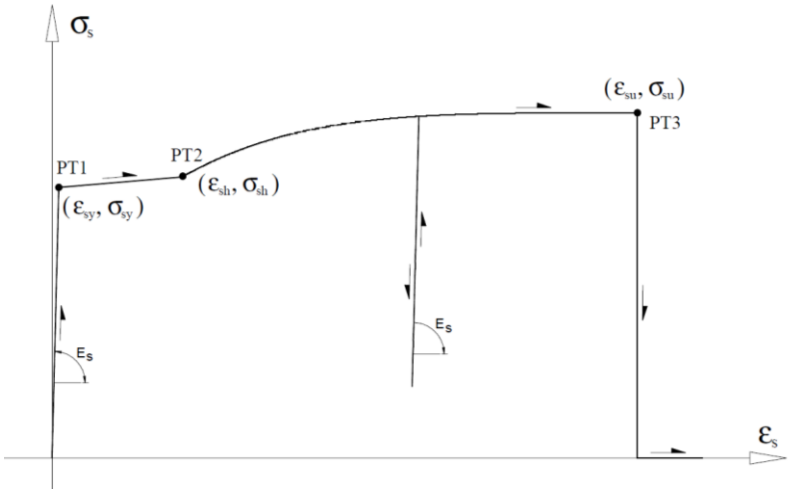

Figure 2.7 Uniaxial constitutive model of the steel reinforcements [Sena-Cruz, 2004]

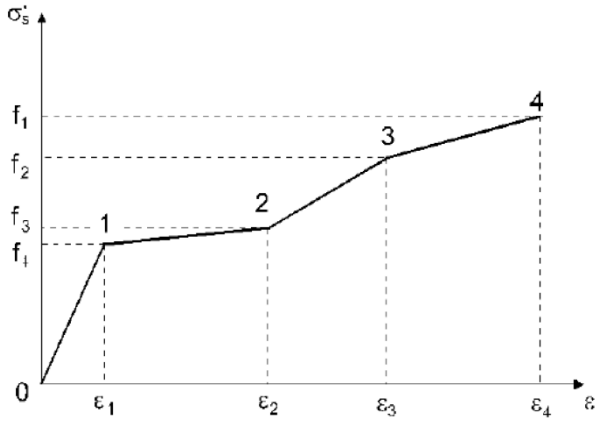

Figure 2.8 Multi-linear stress strain law for steel reinforcement [Chin et al., 2012]

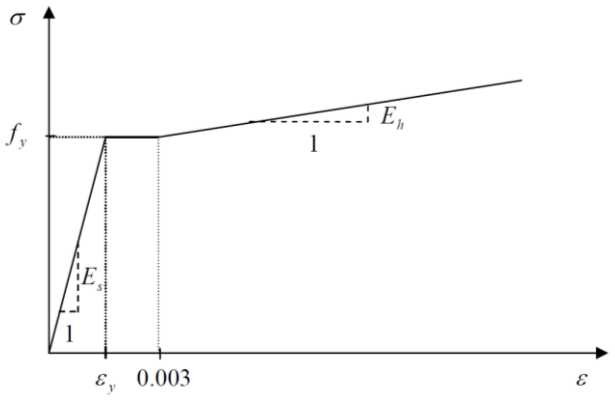

Figure 2.9 Simplified multi-linear stress strain relationship for steel reinforcements [Corrales, 2005]

2.2.3 CFRP Composites

For a unidirectional CFRP laminate in tension, a linear elastic constitutive relation is assumed as illustrated in Figure 2.10. A rupture point on the stress strain relationship for the fiber direction defines the ultimate stress and strain of the CFRP. The Young's modulus is obtained from the constitutive stress strain relation. [Corrales, 2005; Godat et al., 2010; Sena-Cruz et al., 2011; Chin et al., 2012; Michels et al., 2014]

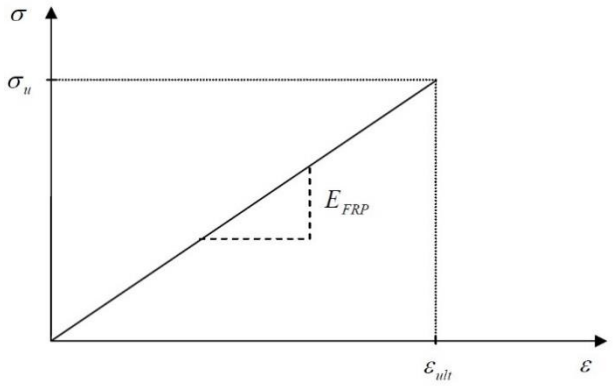

Figure 2.10 Linear elastic stress strain relation for CFRP laminate

2.2.4 Interface Bond Behavior

For reinforced concrete members strengthened with CFRP laminates under shear and flexural, besides conventional concrete failure or CFRP fracture, debonding of CFRP from concrete substrate is one of the most common failure modes. In fact, debonding can often lead to overall structural failure. The most significant role of the concrete-CFRP interface is to transfer the stresses from the concrete to the externally bonded CFRP laminates. The effectiveness of CFRP strengthening largely depends on this interface bond behavior. Therefore, to achieve successful strengthening, it is critical to investigate the concrete-CFRP interface bond behavior and the corresponding models to be applied in simulations.

The bond stress-slip (τ-s) relationship is the fundamental law to describe the interface behavior of two bonding materials. There are different bond stress-slip law proposed by different researchers, such as cut-off type, bilinear type and elasto-plastic type [Sato et al., 1997;

Lorenzis et al., 2001; Chen and Teng, 2001; Lu et al., 2005]. Such divergence indicates the difficulty in defining a reliable bond stress-slip model for the interface.

Lu et al. [2005] investigated the existing bond-slip models for FRP sheets/plates bonded to concrete using the results of 253 pull tests on simple FRP-to-concrete bonded joints. In particular, a set of three new bond-slip models of different levels of sophistications (as shown in Figure 2.11) proposed in this study, had proven to provide good accuracy for both bond strength and the strain distribution in the FRP plate. The three bond-slip models shown in Figure 2.11 had been proposed based on the predictions of a meso-scale finite element model, where τ (MPa) is the local bond (shear) stress, s (mm) is the local slip, τ_{max} (MPa) is the local bond strength, corresponding to the maximum bond/shear stress experienced by the interface, s_0 (mm) is the slip when the bond stress reaches τ_{max}, s_f (mm) is the slip when the bond stress reduces to zero.

Among the three proposed bond-slip models, the bilinear model has been widely adopted due to its simplification and accuracy [Godat et al., 2010; Chin et al., 2012; Michels et al., 2014]. According to Lu et al.[2005], the parameters governing the bilinear bond-slip model are estimated as follows:

$$\tau_{max} = \alpha \times \beta_w \times f_t \tag{2.1}$$

$$s_0 = 0.0195 \times \beta_w \times f_t \tag{2.2}$$

$$s_f = \frac{2G_f}{\tau_{max}} \tag{2.3}$$

where α = 1.5; f_t is the tensile strength of concrete; G_f is the fracture energy given by $G_f = 0.308 \times \beta_w^2 \times \sqrt{f_t}$; and β_w is the width ratio factor given by $\beta_w = \sqrt{\frac{2.25-b_f/b_c}{1.25+b_f/b_c}}$ where b_f and b_c is the width of FRP plate and concrete prism respectively.

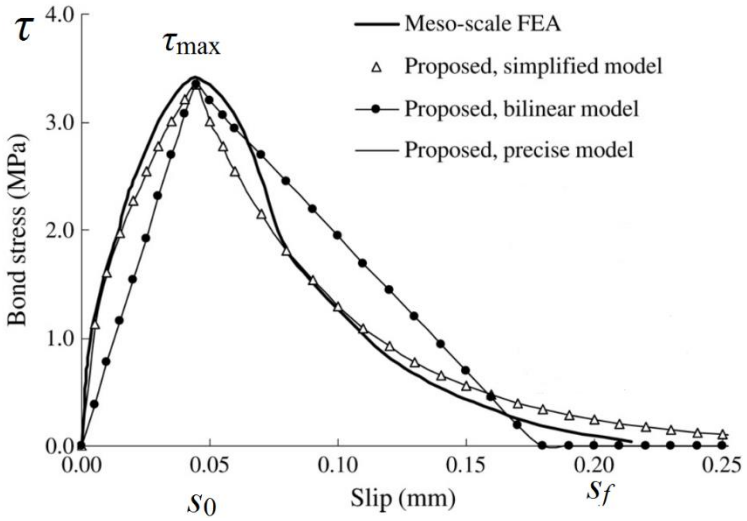

Figure 2.11 Bond-slip curves from meso-scale finite element simulation and proposed bond-slip models

2.3 Research Significance

The research significance of this dissertation is to simulate the experimental results using DIANA finite element analysis software, highlighting the appropriate constitutive material models. In addition, the viscoelastic effect of the strengthened RC slab has been studied via creep analysis. The current work also includes parametric studies, which presents good predictions for several cases of CFRP laminate strengthened RC slabs without physically carrying out the experimental work, saving considerable amount of time, effort and cost. The process of developing these models contributes to the fundamental understanding of finite element analysis for the author.

CHAPTER 3 EXPERIMENTAL RESULTS AND ANALYSIS

3.1 General Information

The experiment data used in the present dissertation was carried out in the scope of the R&D FRPreDur Project (FCT reference - PTDC/ECM-EST/2424/2012). This chapter presents a summary of the work done, highlighting the important aspects for this dissertation. Additional information can be found in Sena-Cruz [2015] and Correia et al. [2015].

3.2 Specimen Geometry and Test Setup

The experimental program was composed of three reinforced concrete (RC) slabs. One slab was used as controlled specimen (REF). One slab was strengthened with a simple CFRP laminate strip according to the EBR technique without any prestressing (EBR). The remaining slab was strengthened with one externally bonded prestressed CFRP laminate strip with a mechanical anchorage (MA). After casting the specimens and before proceed with the application of the CFRP reinforcement, the concrete region of the three slabs where the CFRP was installed were treated by means of sand blasting. The main aim of surface treatment was to remove the weak concrete layer and expose the aggregates to the substrate to ensure sufficient bonding between concrete and CFRP. The cross-sectional geometry of CFRP was 50 mm by length and 1.2 mm by thickness. The initial strain and prestreesing force applied to the CFRP were shown in Table 3.1 below.

The geometry of the specimens and test configuration are shown in Figure 3.1. All slabs have a total length of 2600 mm, being the cross-section of width 600 mm and height 120 mm. The upper and lower longitudinal inner reinforcement is composed of three steel bars with a diameter of 6 mm (3Ø6) and five steel bars of a diameter of 8 mm (5Ø8), respectively. Transverse reinforcements were installed by means of steel stirrups with a diameter of 6 mm (Ø6) spaced at 300 mm. The length of CFRP laminate strips used were 2200 mm.

Monotonic tests up to failure were performed using a four point bending configuration in order to access the service and ultimate behavior of all slabs, being the shear span equal to 900 mm. The two supports were located at 100 mm away from the extreme ends of the slab.

Five linear variable differential transducers (LVDT1 to LVDT5) were used to record the deflection along the longitudinal axis of the slab; 3 strain gauges (SG1 to SG3) to measure the strain in the laminate and concrete; and 1 load cell to measure the applied load (F). Figure 3.1 shows the position of each LVDT: three in the pure bending zone with the range of ±75 mm and a linearity error of ±0.10% and two between the supports and the applied load points with a range of ±25 mm and the same linearity error. The load cell used has a maximum measuring capacity of 200 kN and a linear error of ±0.05%. Two different strain gauge types were used: (i) two TML BFLA-5-3 strain sensors (SG1 and SG2) glued on the laminate surface at the mid-span and at the force application point; and, (ii) one TML PFL-30-11-3L strain sensor (SG3) for the measuring the concrete strain in the mid-span. All tests were carried out with a servo-controlled equipment under displacement control at a rate of 1.2 mm/min. The crack width evolution was measured during the test through a handheld USB microscope which consists of the VEHO VMS-004 D microscope, with a native resolution of 640 × 480 pixels and magnification capacity up to 400×. In this experimental program, the crack width acquisition was done with a magnification factor of 20× up to predefined applied load.

It should be highlighted that, usually, in reality for existing structures cracks already exist at the point of the CFRP application. Consequently, the present experimental program does not totally reproduce the major part of the existing structures that require upgrading. However, critical aspects such as post-cracking behavior, yielding of the longitudinal reinforcements, ultimate load and failure modes can be well-captured by the present experimental program. Hence, the structural behavior of the slabs can be considered representative of the expected real behavior. Additionally, it is also possible to evaluate the effect of the CFRP prestressing on crack initiation from this experiment.

Table 3.1 Experimental program

Specimen	**Laminate geometry [mm^2]**	**Initial strain, ε_{fp} [×10^{-3}]**	**Prestress force [kN]**	**Anchorage system**
REF	-	-	-	-
EBR	50 × 1.2	0	-	-
MA	51 × 1.2	4.23	41.6	MA

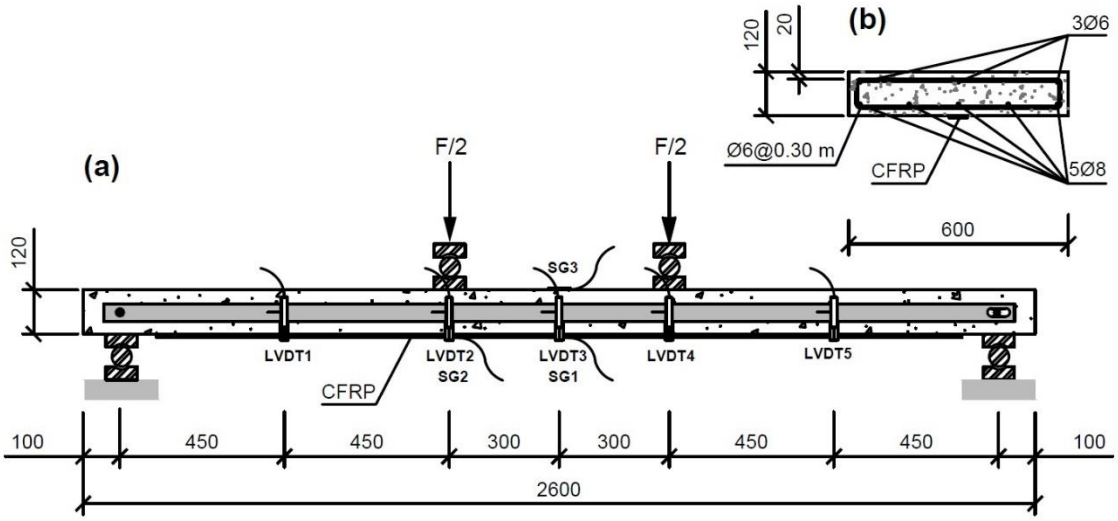

Figure 3.1 Specimen geometry and test setup. (All units are in millimeters)

3.3 Material Characterization

The mechanical properties of the materials involved in the experimental program, namely concrete, steel, CFRP laminate strip and epoxy adhesive, were being evaluated. Concrete characterization included evaluation of the modulus of elasticity (E_c) and compressive strength (f_c) through LNEC E397-1993 [1993] and NP EN 12390-3 [2011] recommendations, respectively. Six cylindrical specimens with 300 mm of height and 150 mm of diameter were used. Table 3.2 shows the results obtained on the testing day. The average compressive strength of concrete was about 40 MPa.

The tensile properties of the steel reinforcement were assessed throughout the NP EN ISO 6892-1[2012] standard. A minimum of three specimens were used for each bar type. Table 3.2 includes the Young's modulus (E_s) as well as the yield (f_y) and ultimate (f_u) strengths obtained from the tensile tests. The average value of the modulus of elasticity was about 207 GPa and 235 GPa for the upper and lower longitudinal steel reinforcement, respectively. The steel of the longitudinal bars and stirrups has a denomination of A400 NR SD according to the NP EN 1992-1-1 [2010].

The CFRP laminate strips used in the experimental work consists of unidirectional carbon fibres held together by an epoxy vinyl ester resin matrix. Typically, this type of CFRP

laminate presents smooth external surface and the fibre volume content is higher than 68% [S&P, 2014]. The modulus of elasticity (E_f) and tensile strength (f_f) were obtained from tests performed according to the ISO 527-5 [1997] standard. The values presented in Table 3.2 are based on the average of six samples and yielded to a mean Young's modulus that varied between 164 GPa and minimum tensile strength of 2375 MPa.

The epoxy adhesive, produced by the same supplier as for the CFRP laminate, was used as bond agent to fix the reinforcements to the concrete substrate. This epoxy adhesive is a solvent free, thixotropic and grey two-component (Component A resin, light grey colour and Component B hardener, black colour). The mixing ratio (A:B) is 4:1 by weight. According to the manufacturer, after mixing the two components, the homogenized compound density is 1.70 to1.80 g/cm^3 and has the following mechanical properties [S&P, 2013]: compressive strength >70 MPa; tensile *E*-modulus >7.1 GPa; shear strength >26 MPa; adhesive tensile strength to concrete or CFRP laminate >3 MPa (after 3 days of curing at 20 ºC). After 7 days of curing at 22 ºC, a Young modulus of 7.7 GPa (CoV 3.1%) and a tensile strength of 20.7 MPa (CoV 9.9%) were obtained [Correia et al., 2015].

Table 3.2 Material characterization (average values)

Concrete	**E_c [GPa]**	**f_c [MPa]**		
	30 (n.a)	40.2 (0.7%)		
Steel	**Diameter [mm]**	**E_s [GPa]**	**f_y [MPa]**	**f_t [MPa]**
	6	206.9 (0.4%)	519.4 (6.1%)	670.2 (5.1%)
	8	235.1 (4.6%)	595.9 (4.1%)	699.0 (2.1%)
CFRP	**Geometry [mm^2]**	**E_{CFRP} [GPa]**	**f_f [MPa]**	
	50 ×1.2	164 (3.1%)	2374.9 (2.5%)	

Note: the values in the parentheses are the corresponding coefficients of variation (CoV).

3.4 Anchorage Procedures

The procedures for installation of mechanical anchorage consists of the following main steps [Michels et al., 2015]:

(i) The first step is the surface preparation of concrete substrate where the strip is applied. In this experiment, sandblasting method was used for concrete surface preparation. Afterwards, compressive air was used to clean the treated region of the slab;

(ii) Several holes are drilled to accommodate temporary and permanent bolt anchors. Six M16 8.8 permanent bolt anchors are used to fix each steel anchorage plate. HIT-HY

200-A® chemical bond agent was used to fix the bolts to concrete. Then, aluminum guides are placed in the right position to guide and fix the clamp units;

(iii) The clamp units are placed in-between the guides at each extremity of the slab;

(iv) The epoxy adhesive is prepared according to the requirements included in producer's technical datasheet and the CFRP laminate strip is cleaned with a solvent. Then, the adhesive is applied on the surface of the CFRP laminate as well as on the concrete surface region in contact with the laminate. A minimum of 2 mm of thickness of epoxy was used. The CFRP laminate strip is then placed in its final position and slightly pressed against the concrete substrate;

(v) The clamping units are closed and a dynamometric key is used to tighten the screws of the clamp units with a torque of 170 N m;

(vi) Anchor plates are slightly grinded with sandpaper and cleaned with a solvent before they are installed in their predefined location. The anchor plates of 270 mm × 200 mm × 10 mm, made of hard aluminum, have 6 holes of 18 mm diameter to accommodate the 6 permanent bolt anchors of 16 mm of diameter;

(vii) The aluminum frames are then placed on their predefined locations and fixed against the concrete with the anchors in order to accommodate the hydraulic cylinder for the application of the prestressing;

(viii) Finally, using a manual hydraulic pump, the prestress is applied to the CFRP laminate strip.

After CFRP is being prestressed, a torque of 150 Nm in each bolt anchor of the anchor plates (with a geometry of 270 mm × 200 mm × 20 mm) is being applied to increase the confinement level in this region and hence reducing the probability of the CFRP laminate sliding at the ends. Subsequently, by using additional fixing screws mounted in-between the frame and the clamp units, the prestressing system is being blocked in order to avoid prestress losses during the curing of the epoxy. The strengthening application is concluded after approximately 24 h, since after this time span the epoxy reaches a degree of curing at about 90% [Fernandes et al., 2015]. In the end, the equipment is removed (fixing screws, clamp units, guides and aluminum frames) and the temporary anchors and CFRP laminate outside of the anchor plates are cut off.

3.5 Monotonic Load Test

3.5.1 Deflection

The relationship between the applied force and the mid-span deflection was monitored and the results are shown in Figure 3.2. The strengthening (both non-prestressed and prestressed) increased the stiffness of the RC slab and CFRP strip composite system, and consequently reduced the deflection for the same applied load as compared to the controlled RC slab. This proves that CFRP strengthening is an effective method to enhance the flexural strength against deflection.

It can be observed from Table 3.3 which summarizes the key results that, prestress did not significantly change the stiffness of the elastic phase (K_I). However, substantial differences were observed in the stage after the crack initiation: firstly, cracking (δ_{cr}, F_{cr}) and steel yielding (δ_y F_y) were delayed when compared with the non-prestressing specimens; and the stiffness after cracking (K_{II}) was higher in the strengthened slabs.

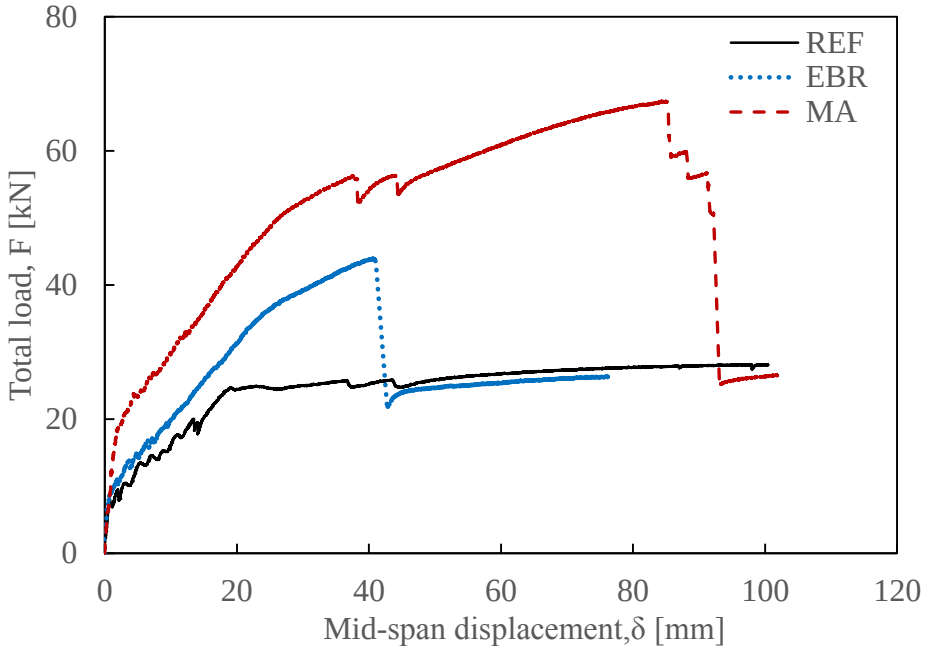

Figure 3.2 Total force versus mid-span deflection

Table 3.3 Main summary of experimental results

Specimen	**Stiffness**		**Crack Initiation**		**Yielding**		**Ultimate**				
	K_I [kN/mm]	K_{II} [kN/mm]	δ_{cr} [mm]	F_{cr} [kN]	δ_y [mm]	ϕ_y [$10^{-3}m^{-1}$]	F_y [kN]	δ_{max} [mm]	F_{max} [kN]	ϕ_{max} [$10^{-3}m^{-1}$]	ε_{fmax}[c] [10^{-3}]
REF	11.10	0.92	0.71	7.88	18.90	-	24.54	100.0[a]	28.07[b]	-	-
EBR	12.49	1.13	0.68	8.49	25.87	43.88	37.05	40.69	43.98	71.34	7.56
MA	9.82	1.31	1.82	17.87	26.88	44.81	50.58	84.78	67.46	77.26	14.76

Note: [a] The slab reached maximum pre-defined deflection without failing
[b] Values for mid-span deflection of 100 mm
[c] The maximum CFRP strain did not necessarily occur at the mid-span

3.5.2 Influence of Prestress

The overall behavior of the prestressed specimens was considerably more satisfying than the un-prestressed ones in terms of ductility and load carrying capacities. Prestressing clearly improved the cracking and yielding initiation, stiffness and load carrying capacity. Even though the stiffness at the uncracked stage (K_I) was similar (prestressed versus un-prestressed) mainly due to the low level of strengthening ratio and level of prestrain that has been used, the cracking load was significantly higher. Similar observations can be made for the cracked stage (before yielding initiation). The load carrying capacity of prestressed slabs increased when compared with the unprestressed specimen.

Figure 3.3 and 3.4 illustrate the evolution of the concrete and CFRP strains at mid-span with the total force, respectively. It shows a higher ultimate strain in the concrete for the prestressed specimens. Consequently, it can be stated that prestressing the CFRP laminates not only improved the slabs overall performance but also assured a better use of the materials. It should be also referred that a greater portion of the CFRP tensile capacity was mobilized with the prestress (see Figure 3.4 and Table 3.3): the strain at the ultimate load (F_{max}) for the MA was 95% higher than the results observed on the EBR.

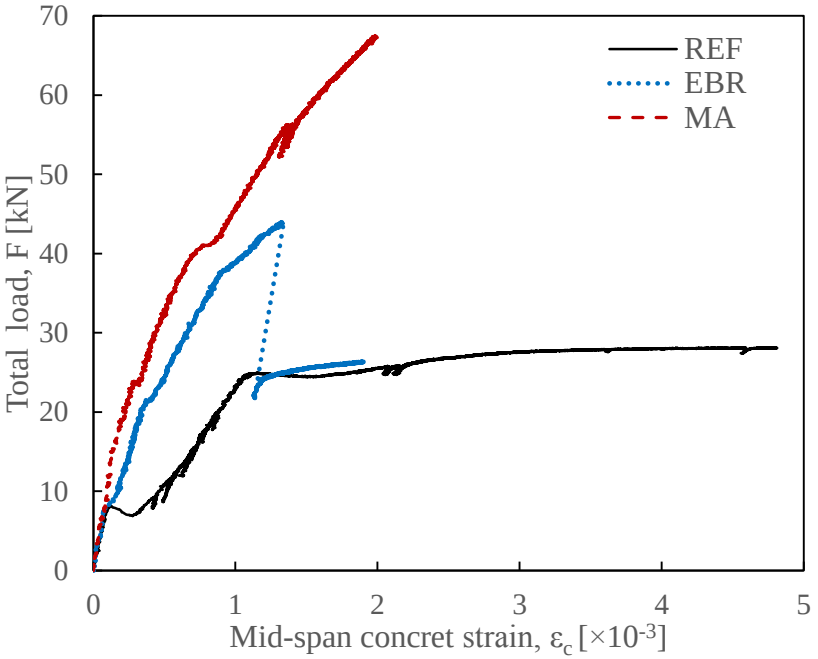

Figure 3.3 Total force versus mid-span concrete strain

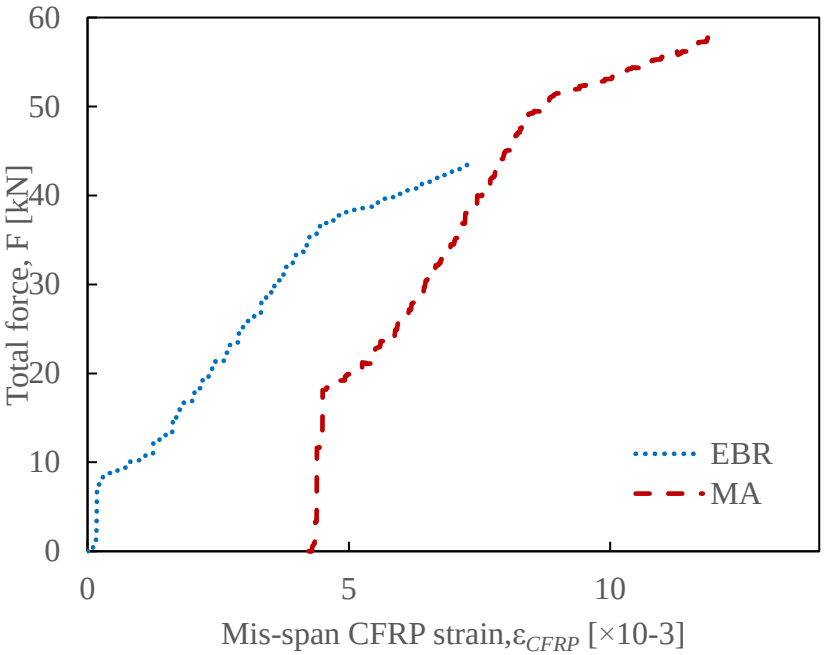

Figure 3.4 Total force versus mid-span CFRP strain

3.6 Creep Test

During the experiment program, creep tests were carried out on the MA slabs to investigate its long-term structural behavior under sustained load. The loading configuration is illustrated in Figure 3.5 and the time history of the slab is summarized in Table 3.4. A sustained

load of 20 kN was applied on 17-Dec-2014 and only the mid-span deflection was measured against time until the end of the creep test on 1-Sep-2015. It should be noted that the ambient temperature was not controlled for the first 350 hours of the creep test. The slab was only submitted to the controlled environment (20ºC and 50% RH) after 350 hours from the beginning of the creep test.

The mid-span deflection of the slab *versus* time during creep test is shown in Figure 3.6. The instantaneous mid-span displacement of the MA slab after the load was being applied was approximately 6 mm. Then the mid-span deflection gradually reached a constant value of approximately 11 mm at about 190 days of creep test. The mid-span deflection after 190 days remained almost constantly at 11 mm until the end of the creep test.

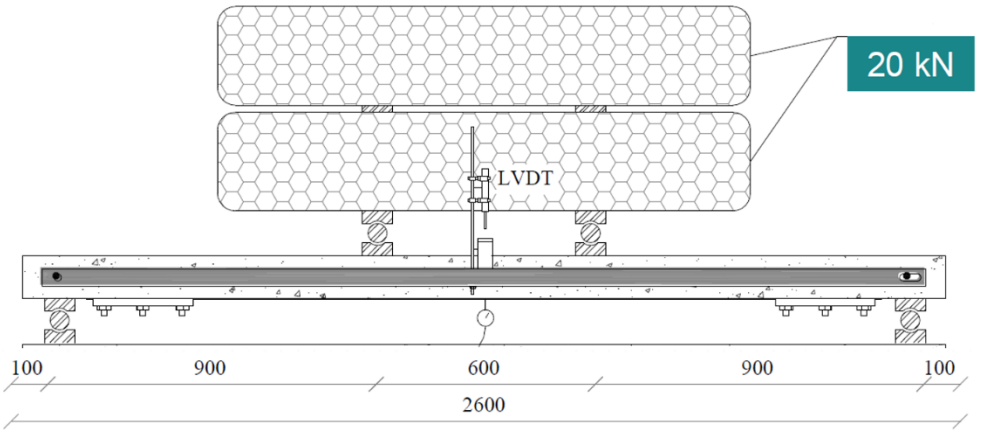

Figure 3.5 Testing configuration for the creep test

Table 3.4 Time history of the MA slab for creep test

Date	Event	Age [day]
11-Apr-2014	Casting concrete slab	0
9-May-2014	Material characterization	28
28-Jun-2014	Strengthening/Prestressing	78
17-Dec-2014	Beginning of creep test	250
1-Sep-2015	Unloading	507

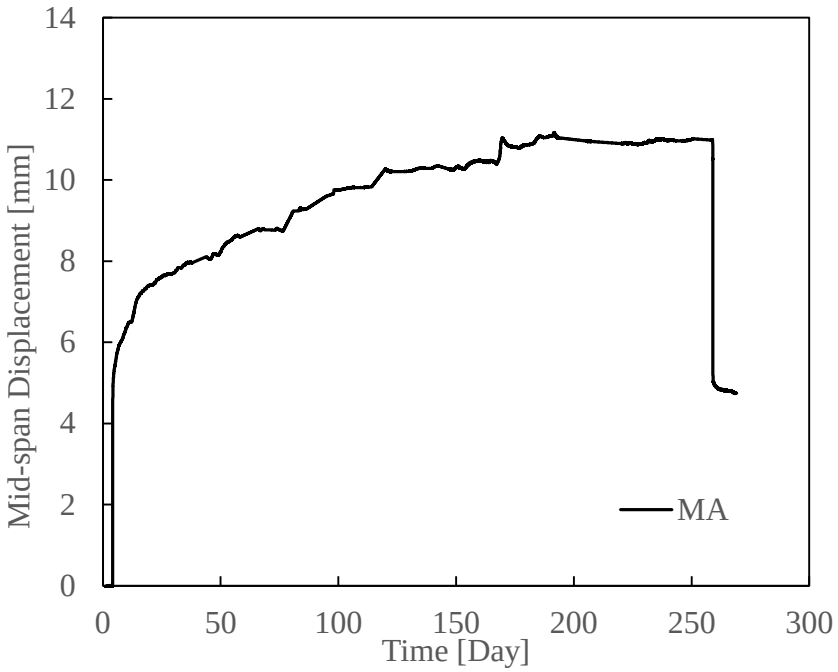

Figure 3.6 Mid-span deflection versus time for MA slab under creep test

3.7 Conclusions

The main objective of the experiment is to assess the service and ultimate behavior of the RC slab strengthened with prestressed CFRP laminate strips according to EBR techniques. In addition, creep test aims to investigate the long-term behavior of the strengthened slab under sustained load. From the work carried out and described in the present chapter, several conclusions could be drawn based on the experimental results.

At service level, strengthening with CFRP (both prestressed and non-prestressed) improved the performance of the slabs in terms of lower deflection, crack width delay and lower crack spacing. In addition, the metallic anchors composing the MA system prevented a premature failure by debonding and allowed the slabs to support higher ultimate loads and deflections. A greater use of the CFRP laminate strip tensile capacity was attained when prestressing was applied to the CFRP laminates. The average ultimate strain on the CFRP laminate increased by 74% with prestressing for the slabs tested.

CHAPTER 4 FINITE ELEMENT MODELLING

4.1 Introduction

Finite element simulation of the slabs is carried out using the commercial finite element software DIANA 9.6, which is well known for modeling concrete structures due to its wide range of concrete materials models and advanced numerical tools. The non-linear mechanisms that are considered in modeling are cracking of concrete, yielding of reinforcement and the debonding (or failure) of the CFRP laminate. All the finite element models in this study are two dimensional assuming plane stress state. iDIANA is mainly used for pre-processing and post-processing of the models, while Command Box is used to run the analysis.

4.1.1 Model Geometry

Three reinforced concrete (RC) slabs were being tested under four-point bending test configuration. One RC slab was used as controlled specimen (REF). One RC slab was strengthened with a simple CFRP laminate strip according to the EBR technique without any prestressing (EBR). The remaining slab was strengthened with one externally bonded prestressed CFRP laminate strip with a mechanical anchorage (MA). All slabs have a total length of 2600 mm, the rectangular cross section of width 600 mm and height 120 mm. The CFRP laminates is located at 200 mm away from two ends, having an effective length of 2200 mm (Figure 4.1). The detailed geometry about the slabs are descripted in Chapter 3 section 3.2 Specimen geometry and test setup.

Due to the symmetry of the test configuration, half of the slab is used for numerical simulation, reducing the computing time considerably. Figure 4.2 shows the geometrical model of REF slab, while Figure 4.3 shows the ones for the case of slabs with EBR and MA respectively. Note that for the strengthened slabs (EBR and MA), there is a 2mm thickness of interface between the bottom surface of concrete slab and CFRP.

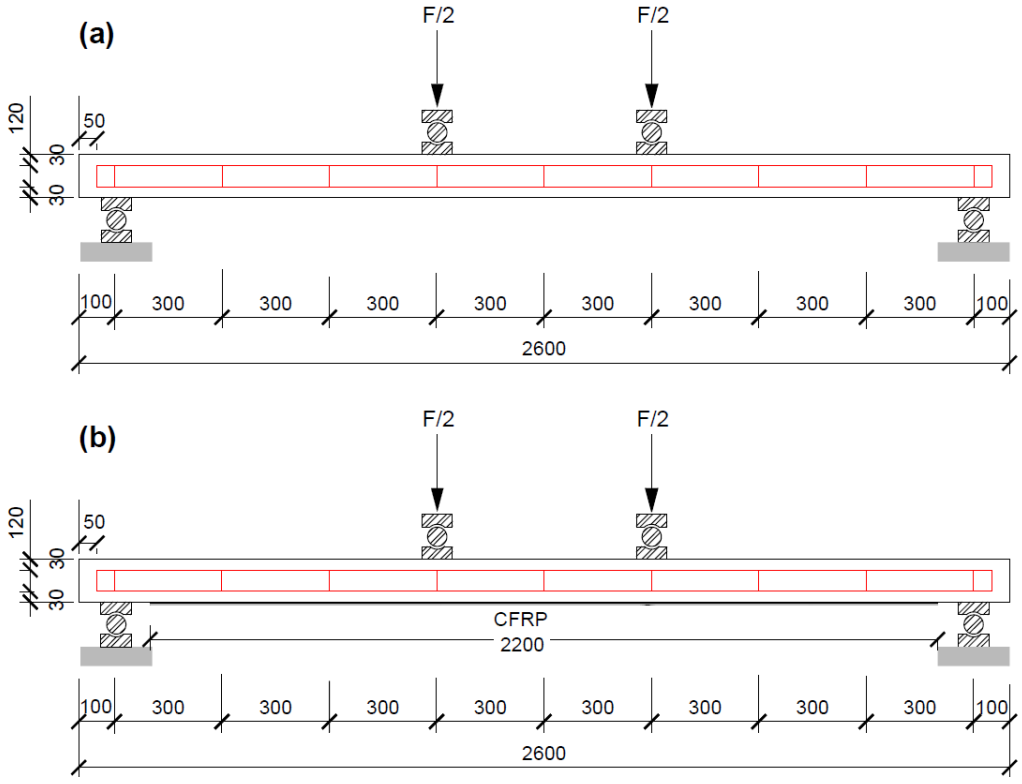

Figure 4.1 Geometry details of (a) REF slab and (b) strengthened (EBR and MA) slab (All units in milimeter)

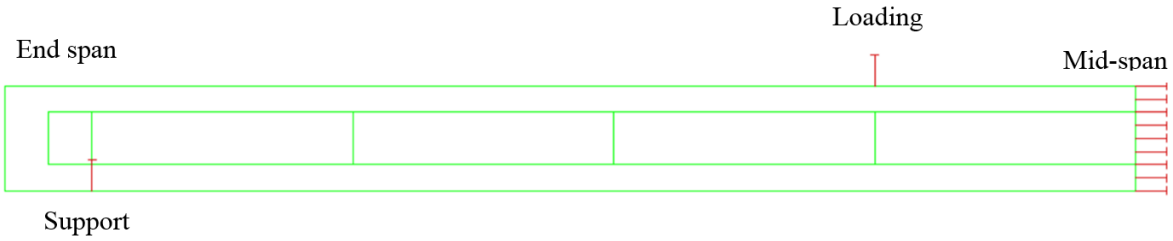

Figure 4.2 Geometrical model of the reference slab (REF)

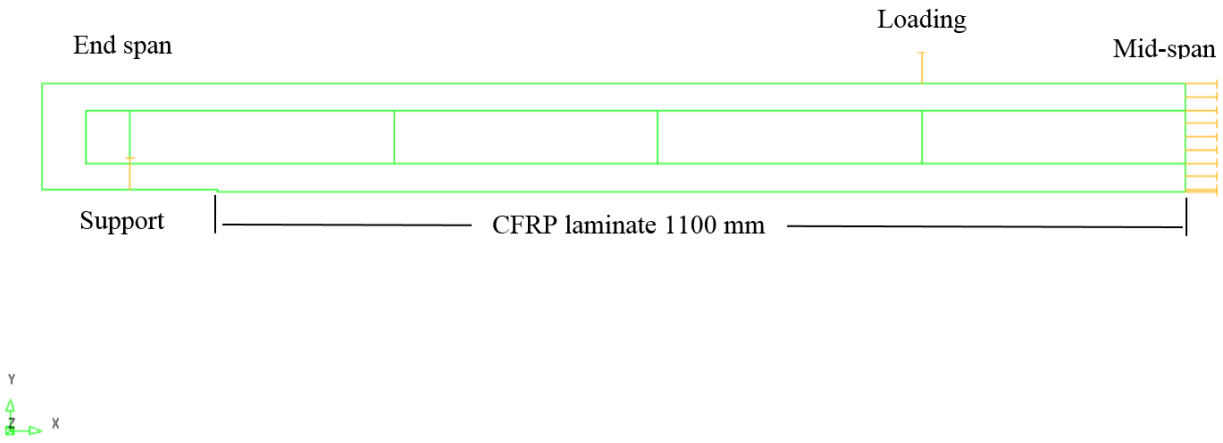

Figure 4.3 Geometrical model of strengthened slab (EBR and MA)

4.1.2 Element Meshes

Rectangular finite element of 25 mm × 15 mm were used for modeling the concrete component of all slabs. The number of elements used to mesh concrete and steel reinforcement are kept constant. Table 4.1 shows the number of elements used to model each constitutive material of the model for the three slabs.

Table 4.1 Summary of number of elements used in the models

	Number of elements		
	REF	**EBR**	**MA**
Concrete	416	416	416
Steel reinforcement	124	124	124
CFRP laminate	-	44	44
Interface	-	44	44

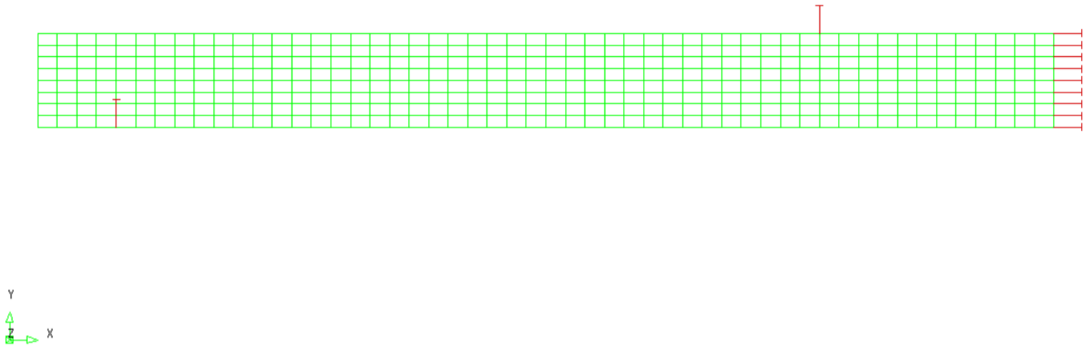

Figure 4.4 Mesh for reference slab (REF)

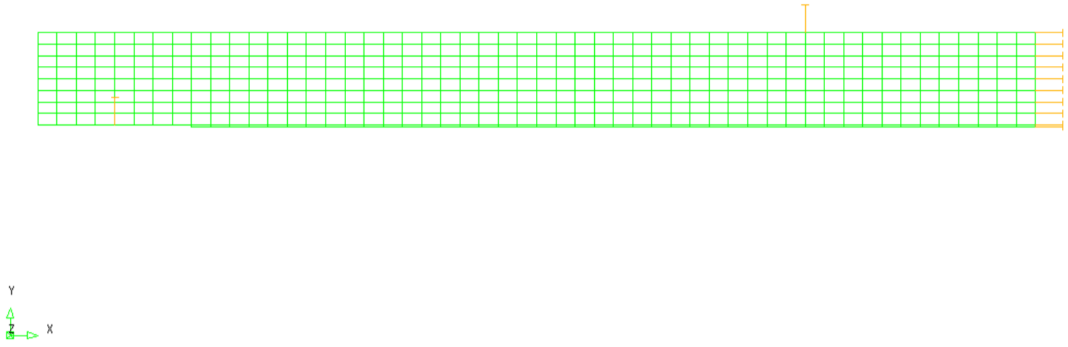

Figure 4.5 Mesh for strengthened slabs (EBR and MA)

4.1.3 Element Types

There are a total of four different element types used in this study. The selection of element type was based on various circumstances, such as mesh typology, boundary conditions and property assignment. Table 4.2 summarizes all the element types used in the model. The details of element type for each material will be elaborated in the following subsections.

Table 4.2 Summary of element types used in the model

Material	Element type	DIANA syntax
Concrete	Quadrilateral isoparametric plane stress element	QU4 Q8MEM
Steel	Embedded reinforcement	REINFORCE BAR
CFRP laminate	Regular truss element	BE2 L2TRU
Interface	Double line element 2+2 nodes	IL22 L8IF

4.1.3.1 Concrete

Concrete is discretized using quadrilateral element QU4. QU4 is defined by 4 nodes connected by 4 straight lines within a specified element. The element type for the model is Q8MEM as illustrated in Figure 4.6. The Q8MEM element is a four-node quadrilateral isoparametric plane stress element. It is based on linear interpolation and Gauss integration [DIANA, 2015]. The polynomial for the displacements u_x and u_y can be expressed as

$$u_i(\xi,\eta) = a_0 + a_1\xi + a_2\eta + a_3\xi\eta$$

Typically, this polynomial yields a strain ε_{xx} which is constant in *x* direction and varies linearly in *y* direction and a strain ε_{yy} which is constant in *y* direction and varies linearly in *x* direction. For constant shear, the Q8MEM element yields a constant shear strain γ_{xy} over the element area. By default DIANA applies 2 × 2 [$n_\xi = 2$, $n_\eta = 2$] integration, 1 x 1 is a suitable option for which DIANA applies a stabilization procedure to avoid zero-energy modes. Schemes higher than 2 × 2 are not suitable.

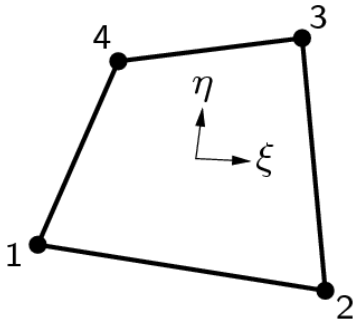

Figure 4.6 Q8MEM element type [DIANA, 2015]

4.1.3.2 Steel Reinforcement

All the steel reinforcement are modeled as embedded reinforcement which does not allow relative slip between steel and concrete. They are represented as lines in a two-dimensional finite element model. In DIANA, the space occupied by embedded reinforcements is ignored. The embedded reinforcements do not contribute to the weight of the whole model. Since embedded reinforcements do not allow relative slip, they have no degree of freedom on

their own. In addition, the strains in the reinforcements are computed from the displacement field of the concrete element. This implies that there is perfect bond between the reinforcement and concrete.

In this study, there are two types of steel, with diameters of 6 mm (Ø6) and 8 mm (Ø8), being used. Ø6 steel bars are used as upper longitudinal reinforcement and shear reinforcement, while Ø8 steel bars are used as bottom longitudinal reinforcement. The material characterization and detailing information are elaborated in details earlier in Chapter 3. These steel reinforcement bars are generated by locating the start and end points within the concrete element using global coordinates. Subsequently, the steel reinforcement are assigned with their respective material properties.

4.1.3.3 CFRP Laminate

In this dissertation, regular truss element is used to model CFRP laminates. In DIANA, there are three types of truss elements available: regular, enhanced and cable elements. Enhanced and cable elements are suitable for higher degree of freedom perpendicular to the bar or element axis as shown in Figure 4.7. Moreover, the deformation of truss elements can only be the axial elongation Δl, without bending nor shear deformation. According to DIANA manual, truss elements are bars which must fulfill the condition that the dimensions d perpendicular to the bar axis are small in relation to the length l of the bar as shown in Figure 4.7. In the experiment, the thickness of the slab is 120 mm and it is considered rather small in relation to the length of CFRP laminates are 2200 mm for the whole slab (or 1100 mm for half the slab). In addition, CFRP laminates are bonded to the bottom surface of the slabs, either as externally bonded reinforcement (EBR), or by means of mechanical anchorage (MA), there is no degree of freedom in the direction perpendicular to the CFRP laminates. Therefore, regular truss element is adopted to model CFRP.

The truss element types are represented as lines in DIANA. In this study, the L2TRU is used as element type for CFRP (Figure 4.8). L2TRU has linear interpolation functions for the displacement field u_x, meaning that there are only two nodes along the line for regular truss element. This element type yields a constant strain along the bar axis.

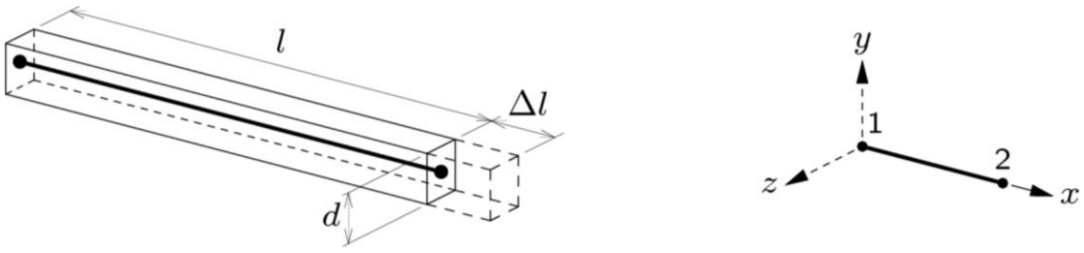

Figure 4.7 Characteristic of truss element [DIANA, 2015]

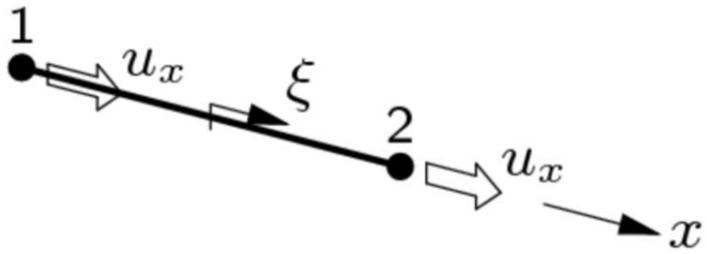

Figure 4.8 L2TRU element type with 2 nodes in a straight line [DIANA, 2015]

4.1.3.4 Interface

The interface elements describe the interface behavior in terms of a relation between the normal and shear tractions and the normal and shear relative displacements across the interface. There are several typical applications of structural interface elements, such as elastic bedding, bond-slip along reinforcement, friction between surfaces and masonry joints. According to DIANA 9.6 user manual [2015], there are four types of structural interface elements available with respect to shape and connectivity: nodal interface elements, line interface elements, line-solid connection interface element and plane interface elements. In this study, line interface element which is to be placed between truss element and concrete plane stress element in a two-dimensional model, is most suitable to model the concrete-FRP interface.

Since the element type used for CFRP laminate has two nodes in a straight line, the element type for concrete-CFRP interface should match the number of nodes per line with that of CFRP laminate. Therefore, L8IF which is an interface element between two lines in a two-dimensional configuration is chosen as the interface element type (Figure 4.9). For L8IF interface element, the local *xy* axes for the displacements are evaluated in the first node with *x* from node 1 to node 2.

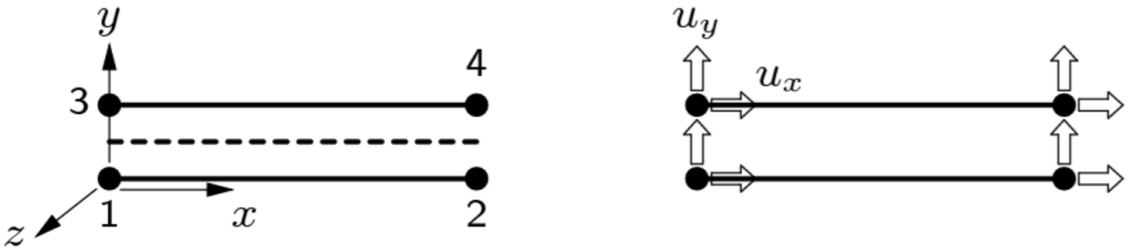

Figure 4.9 L8IF element typology (left) and displacements (right)

4.1.4 Boundary Conditions

All slabs under four-point bending test were simply supported. Due to the symmetry effect of loading and slab geometry, only half of the actual slab was modeled. In the model, the left support provides constrain of translation in y-direction, located at 100 mm from the slab end. Roller support is provided at the mid-span to restrict translation in x-direction and allow translation in y-direction as shown in Figure 4.2 and 4.3.

4.1.5 Loading Conditions

The actual four slabs were subjected to two concentrated static loads applied at 600 mm apart (as shown in Figure 4.1). In the model which is half of the actual slab, the loading point is located at 300 mm away to the mid-span. During the experiment, all tests were carried out with a servo-controlled equipment under displacement control at a rate of 1.2 mm/min. The ultimate load capacity of the slabs and displacement at mid span were measured. The experimental results and analysis were elaborated in details in Chapter 3. It was observed from the experiment that the maximum mid-span deflection for slabs were approximately 100 mm. In order to simulate the test condition, a prescribed displacement of 100 mm was assigned as the load condition to the model.

In a non-linear analysis for a finite element model, the load is not applied all at once, but it is incrementally applied in a specified number of "load steps". Load steps are explicitly determined by the user in the command file. In each load step, a system of nonlinear equations are being solved. At the end of each incremental solution, the global stiffness matrix is modified to take into account the nonlinear behavior of the materials before going to the next increment.

Regular Newton-Raphson iterative solution method is used to obtain convergence between internal and external forces in the model and then the displacement vectors.

The load steps applied in the model are not of the same magnitude. This is due to the fact of nonlinear behavior of the materials used, mostly concrete. From the experimental load-displacement curve result, there are a few distinguished nonlinear behavior observed. These marked points are corresponding to mechanical behaviors of the slabs during testing, such as first crack, steel yielding, interface debonding and concrete crushing and so on. The load step size is significantly reduced around these parts in order to obtain representative behaviors and avoid divergence.

Once the analysis is complete, the load-step increment curve can be obtained from the left support element node. The displacement-step increment curve can be obtained from the loading point element node. The total load applied to the slab and the corresponding displacement can therefore be plotted through force-displacement graph. Moreover, total applied force versus the bottom longitudinal steel reinforcement strain at mid-span is also captured for all four slabs. This information enables us a better understanding of the tensile behavior and thus the maximum tensile strain experienced by the bottom longitudinal steel reinforcement which could not be easily measured during experimental process. In addition, the total applied force versus top concrete strain at mid-span is monitored and compared with experimental results for all four slabs. The total applied force versus CFRP strain at mid-span is also captured and compared with experimental results for all slabs except for the REF slab. Finally, the numerical crack patterns obtained at the final step are mapped with the ones observed during the experiment.

4.2 Constitutive Material Model Properties

In a finite element analysis, one of the most difficult task is probably to accurately predict the material models to be used, especially for the case of nonlinearity of the material. There are a total of four different materials used in the finite element model, namely: concrete, steel reinforcement, CFRP laminates and CFRP-concrete interface. In this study, there are mainly two procedures to evaluate and define the respective material models. Firstly, the basic

material properties can be obtained from experimental testing as presented in Chapter 3. In addition, empirical equations or recommendations from published literatures have been adopted as well. In some cases which is difficult to get an accurate behavior of the material, some assumptions have to be made and will be discussed in details in the following subsections.

4.2.1 Concrete

Concrete is a heterogeneous, cohesive-frictional material and exhibits non-linear inelastic behavior under multi-axial stress states in real life. Concrete contains many micro-cracks, especially at the interface between aggregates and mortar, even before application of external loads. There are many theories proposed in the literatures to predict the concrete behavior in nonlinear analysis. One of the most challenging tasks in a finite element analysis is to simulate concrete in a nonlinear analysis. Table 4.3 summarizes the material model adopted for concrete in this study. The following subsections will explain in details about each property.

Table 4.3 Summary of concrete material model properties

Property	**Remarks**	**DIANA syntax**
Young's modulus, E_c	30 GPa	YOUNG 3.00E+4
Poisson ratio	0.2	POISON 0.2
Compressive strength, f_{cm}	40 MPa	-
Tensile strength, f_t	2 MPa	-
Crack model	Multi-directional fixed crack	-
Tension cut-off	Constant	CRACK 1
Tension softening	Hordijk et al,.	TENSIO 5
Fracture energy, G_f	0.07 N/mm	GF 0.07
Crack bandwidth, h	30 mm	CRACKB 30
Shear retention	Full shear retention	TAUCRI 0

4.2.1.1 Multi-directional fixed crack model

In this study, multi-directional fixed smeared crack model is used for concrete under nonlinear analysis. In a multi-directional fixed smeared crack model, cracking is specified as a combination of tension cut-off, tension softening and shear retention. The fundamental feature of the smeared crack model is the decomposition of the total strain ε into a concrete strain ε^{co} and a crack strain ε^{cr} as

$$\varepsilon = \varepsilon^{co} + \varepsilon^{cr} \tag{4.1}$$

An advantage of such total strain decomposition is that it allows for a further sub-decomposition of the crack strain into its contributors from a series of multi-directional cracks that simultaneously occur as

$$\varepsilon^{cr} = \varepsilon_1{}^{cr} + \varepsilon_2{}^{cr} + \ldots\ldots \tag{4.2}$$

where $\varepsilon_1{}^{cr}$ is the global crack strain increment owing to a primary crack, while $\varepsilon_2{}^{cr}$ is the global crack strain increment owing to a secondary crack and so on. The sub-decomposition of the crack strain ε^{cr} gives the possibility of modeling a number of cracks that simultaneously occur. The significant feature of this multi-directional fixed crack concept is that a stress σ_i and strain $\varepsilon_i{}^{cr}$ exists in the *n -t* coordinate system that is aligned with each crack *i* as illustrated in Figure 4.10. Whenever the angle of inclination between the existing crack(s) and the current direction of principal stress exceeds the value of a certain threshold angle α, a new crack is initiated. As such, a system of non-orthogonal cracks is implied as pioneered by de Borst and Nauta [1985].

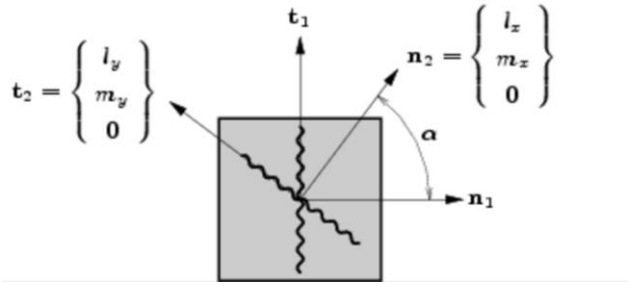

Figure 4.10 Multi-directional fixed crack model

4.2.1.2 Tension cut-off

Tension cut-off is one factor that governs the crack initiation and propagation. There are two tension cut-off criteria available in DIANA: constant and linear, as shown in Figure 4.11. Tension cut-off criterion implies that cracks occur when the principal tensile stress violates the maximum stress condition. For instance, constant stress cut-off implies that a crack arises if the major principal tensile stress exceeds tensile strength f_t which is the controlling strength to determine crack initiation. A linear stress cut-off implies that a crack arises if the

major principal tensile stress exceeds the minimum of f_t and $f_t\,(1 + \sigma_{lateral}/f_c)$, with $\sigma_{lateral}$ the lateral principal stress and f_c the compressive strength.

In this study, a constant stress cut-off criteria has been adopted. The tensile strength f_t was not experimentally determined, but estimated based on formulations recommended by CEB-FIB [1990] as follows:

$$f_{ct,mean} = 0.3 \times f_{ck}^{\frac{2}{3}} \tag{4.3}$$

where $f_{ck} = f_{cm} - 8MPa$, with f_{cm} equals to 40 MPa as determined from the experiment. However, when the tensile strength f_t estimated from Equation (4.3) which is about 3 MPa was used as the stress cut-off criteria, it has been noted that the overall behavior of the model has been overestimated. Due to this observation, a tensile strength value of 2 MPa has been adopted in the analysis.

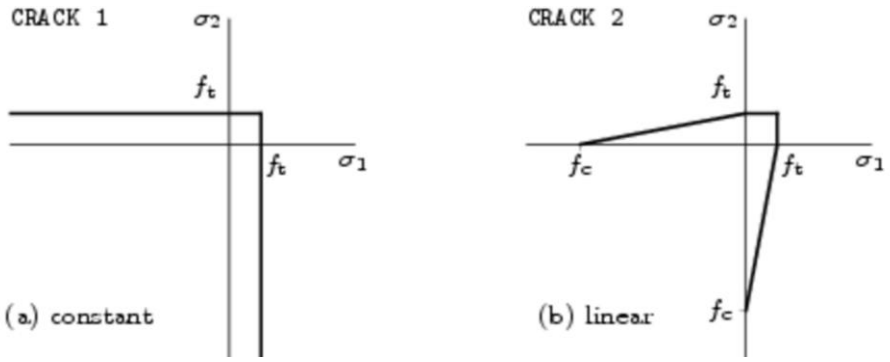

Figure 4.11 Tension cut-off in 2-dimensional principal stress space

4.2.1.3 Tension softening

The relation between the crack stress σ_{nn}^{cr} and the crack strain ε_{nn}^{cr} in the normal direction can be written as a multiplicative relation

$$\sigma_{nn}^{cr}\,(\varepsilon_{nn}^{cr}) = f_t \times y\,(\frac{\varepsilon_{nn}^{cr}}{\varepsilon_{nn.ult}^{cr}}) \tag{4.4}$$

in which f_t is the tensile strength and $\varepsilon_{nn.ult}^{cr}$ the ultimate crack strain. The general function y represents the actual softening diagram. In DIANA both the tensile strength and

ultimate strain may be a function of temperature, moisture concentration or maturity. Therefore the development of tensile strength and fracture energy in time can be simulated.

In this study, among all eight available tension softening models in DIANA, a nonlinear tension softening according to Hordijk et al.[1987] , which has been adopted by many researchers [Chin et al., 2012; Correlas, 2005], is used. This model proposed an expression for the softening behavior of concrete which also results in a crack stress equal to zero at a crack strain $\varepsilon_{nn.ult}^{cr}$ as shown in Figure 4.12.

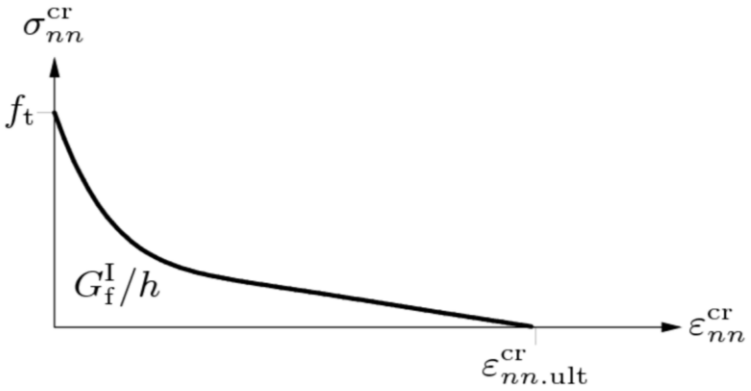

Figure 4.12 Nonlinear tension softening [Hordijk et al., 1987]

Fracture energy G_f is estimated according to Equation (4.5) as specified in CEB-FIP Model Code [1990] which provides relationship between compressive strength and fracture energy. The fracture energy is related to both the compressive strength f_{cm} and the maximum aggregate size d_{max}. The relationship according to the Model Code is:

$$G_f = G_{f0} \left(\frac{f_{cm}}{f_{cm0}}\right)^{0.7} \tag{4.5}$$

with f_{cm0} equal to 10 MPa and the value of G_{f0} related to the maximum aggregate size (Table 4.4). The maximum aggregate size used in concrete slabs is 12.5 mm, and thus the G_{f0} value is interpolated as 0.0275.

Table 4.4 Coefficient for determining fracture energy [MC 1990]

Maximum aggregate size, d_{max} [mm]	Fracture energy, G_{f0}[N/mm]
8	0.025
16	0.03
32	0.058

In the smeared crack approach, the fracture zone is distributed in a certain width of the finite element, which is designated crack band-width, *h*. The crack band-width must be mesh dependent in order to ensure mesh objectivity [Sena-Cruz, 2004]. There are several different ways to estimate *h*. In this study, the relationship $h = \sqrt{2 \times A}$ is used to estimated crack bandwidth, where *A* is the area of a single element mesh.

4.2.1.4 Shear retention

When a crack occurs, the shear stiffness of the material is usually reduced. This reduction is generally known as shear retention. DIANA offers two predefined relations for shear retention: full shear retention and constant shear retention. The crack secant shear stiffness is given by the general relation:

$$D_{secant}^{II} = \frac{\beta}{1-\beta} G \tag{4.6}$$

where *G* is the elastic shear modulus, β is the shear retention factor.

In case of full shear retention, the elastic shear modulus *G* is not reduced, and thus β =1 which implies that the secant crack shear stiffness is infinite. In case of constant shear retention, the crack secant shear stiffness is reduced, the shear retention factor is in the range of $0 < \beta \leq 1$. In this study, full shear retention is used in the model.

4.2.2 Steel Reinforcement

For embedded reinforcement, DIANA offers seven different material models [DIANA, 2015]. Among all the available material models, Von Mises plasticity and hardening model is adopted for embedded reinforcement in the present study. Figure 4.13 illustrates the bilinear stress strain relationship diagram for the embedded reinforcement. The yield stress f_y and ultimate stress f_{ult} are measured from the experimental testing of steels. The Young's modulus used in the finite element model for both Ø6 and Ø8 steels are not the ones determined from the experimental testing, but assumed to be 200 GPa. The yield strain ε_y input in the model is thus obtained from the stress-strain relationship. The ultimate strains ε_{ult} for both types of steels are assumed to be 0.1. The Poisson ratio is specified as 0.3 for the steel reinforcement. The main properties for steel reinforcements are summarized in Table 4.5.

Since 2-dimensional model is used to simulate 3-dimensional slab, the cross-sectional areas of the steel reinforcement specified in material properties are the total cross-sectional areas of the steel reinforcement. For instance, three Ø6 steel bars are used as upper longitudinal reinforcement, and thus the cross-sectional areas assigned to it would be the total cross-sectional areas of the three Ø6 steel bars. Therefore, for the same reason, the cross-sectional areas assigned to lower longitudinal reinforcement are the total cross-sectional areas of five Ø8 steel bars. The cross-sectional areas assigned to all shear reinforcement are two times the cross-sectional area of a single Ø6 steel bar, except for the one at the mid span which has the cross-sectional area of a single Ø6 steel bar due to the symmetry effect.

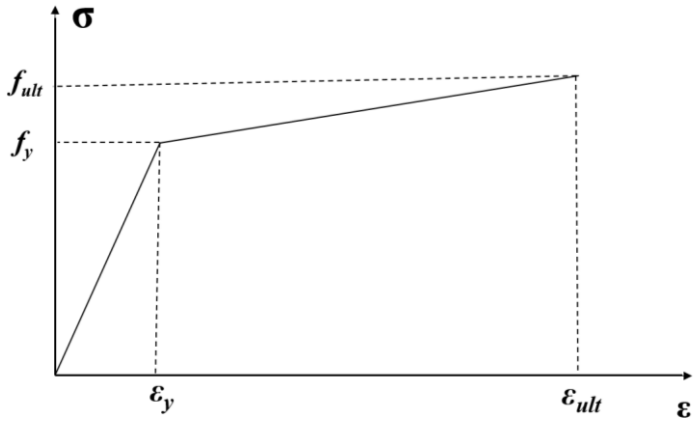

Figure 4.13 Bilinear stress-strain relationship for steel

Table 4.5 Summary of steel reinforcement model properties

Property	Remarks	DIANA syntax
Young's modulus, E_s	200 GPa	YOUNG 2.00E+5
Poisson ratio	0.3	POISON 0.3
Reinforcement model	Von Mises plasticity	YIELD VMISES
Hardening model	Bilinear	HARDIA $f_{y,d}$, $\varepsilon_{y,d}$, $f_{ul,d}$,0.1

However, in the initial analysis in which the yield stress f_y and ultimate stress f_{ult} obtained from the experimental results were used in the model, it was discovered that the finite element model overestimated the results for total applied load versus deflection when comparing with the experimental results. This is due to the fact that the stress-strain relationship for a bare steel reinforcement is different from the average stress-strain relationship for steel

reinforcement embedded in concrete. In another word, the averaged stress-strain relationship for embedded steel reinforcement should have lower yield stress and ultimate stress than those of a bare steel reinforcement. Therefore, to take into account for this fact, the yield envelope of the bare steel reinforcement is reduced as illustrated in Figure 4.14, according to the expression proposed by Stevens et al. [1987]:

$$\Delta\sigma_{ycr} = \frac{75}{\phi_s} f_{ct} \times C_b \tag{4.7}$$

where ϕ_s is the diameter of the steel reinforcement, f_{ct} is the tensile strength of concrete, and C_b is the effective grip factor evaluated from Equation (4.6). A non-perfect grip case is considered in this study.

$$C_b = \begin{cases} 1 \ \text{(perfect grip)} \\ \dfrac{\tau_b}{5f_{ct}}, \tau_b = 13.5 \ \text{MPa} \ \text{(other cases)} \end{cases} \tag{4.8}$$

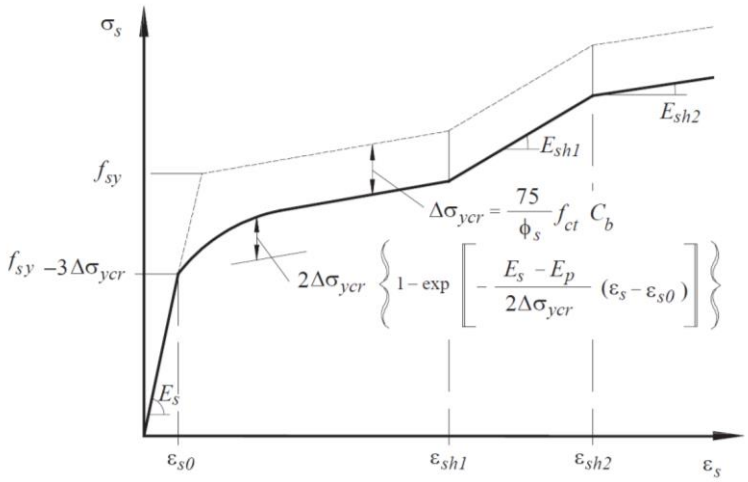

Figure 4.14 The averaged stress-strain relationship for embedded steel reinforcement with reduced yield envelope [Stevens et al., 1987]

4.2.3 Carbon Fiber Reinforcement Polymer (CFRP)

In this experimental work, the CFRP laminate strips consists of unidirectional carbon fibers held together by epoxy vinyl ester resin matrix. The material property of CFRP laminate was characterized and presented in Chapter 3. The Young's modulus of CFRP laminate is 164 GPa. The cross sectional area is 60 mm^2 with a length of 50 mm and a thickness of 1.2 mm.

The behavior of CFRP laminate in all three directions is considered to be linear elastic. A summary of the main properties of CFRP is shown in Table 4.6.

Table 4.6 Summary of CFRP material model properties

Property	Remarks	DIANA syntax
Young's modulus, E_{CFRP}	164 GPa	YOUNG 164E+3
Cross sectional area	60 mm^2	CROSSE 60

4.2.4 Concrete-CFRP Interface

Interface material model is one of the most difficult parts to be determined since there was no experimental work carried out to characterize the interface material property. To simulate the interface behavior in the present study, bond-slip model has been adopted among all the available interface models offered by DIANA. In particular, a bilinear bond-slip law has been proven to be suitable to model unidirectional interface element [Lu et al., 2005]. As shown in Figure 4.15, the maximum bond stress τ_{max} is reached at relative slip s_0 before debonding initiation occurs between CFRP and concrete substrate. The elastic stiffness D_{11} is obtained from the initial slope before debonding point. After τ_{max} is reached and debonding initiation starts, the bond stress decreases linearly to 0 at ultimate slip s_{max}. At this point, complete debonding occurs.

In this study, the recommendation of initial slip at 0.05 mm and ultimate slip at 0.2 mm by Lu et al. [2005] has been adopted. Several attempts were made to evaluate the maximum bond strength τ_{max} within the range of 4 MPa ~7 MPa. It has been found that a τ_{max} value of 6 MPa best correlates the interface behavior in the finite element model with that of experimental results. A summary of main properties for interface is shown in Table 4.7 below.

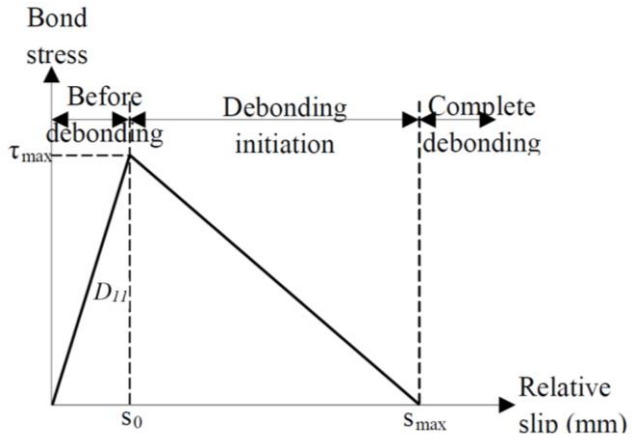

Figure 4.15 The bond-slip model for unidirectional interface element [Lu et al. 2005]

Table 4.7 Summary of interface material model properties

Property	Remarks	DIANA syntax
Maximum bond strength	6 MPa	-
Stiffness	110 MPa/mm	DSTIF 110
Bond-slip	Bi-linear law	SLPVAL 0 0 6 0.05 0 0.2

4.3 Prestressing

The prestress has been applied as a temperature loading to CFRP in the model, following the relationship in Equation (4.9)

$$\varepsilon_{ini} = \alpha \times \Delta t \tag{4.9}$$

where ε_{ini} is the initial strain measured in the prestressed CFRP, α is the thermal expansion coefficient of CFRP and assumed to be 1×10^{-5} $℃^{-1}$ and Δt is the change in temperature. For the RC slab strengthened with CFRP by mechanical anchorage, the initial strain measured in the prestressed CFRP is 4.23×10^{-3}. Thus, a temperature load of -423 ℃ is applied to all the CFRP elements.

In addition, the temperature load which cannot be processed directly in a nonlinear analysis, must be analyzed in the transient state in DIANA. As such, the temperature load is applied at the beginning of the analysis as load case 1, followed by a deformation load as load case 2. In this way, the prestress force is being applied to the CFRP elements first before the nonlinear analysis is being processed.

4.4 Mechanical Anchorage

For the case of MA, the prestressed CFRP laminates were fixed onto concrete by means of mechanical anchor plates (with a geometry of 270 mm × 200 mm × 20 mm). The detailed illustrations and procedures are described in Chapter 3. The length of the mechanical anchor plate is 270 mm. Since there is no information about the effective length of such device, two methods have been attempted to model the anchorage. The mechanical anchorage is simulated by fixing the CFRP laminate to the concrete substrate: (i) over the length of anchor plate (200~300 mm); or (ii) at a single extremity. From several trials, it has been discovered that a single point anchorage best correlates the simulation results with experimental results.

The master-slave approach has been adopted to model the mechanical anchorage as a single point constraint. In this method, the geometric point of the CFRP extremity is being assigned as the "slave" and the corresponding geometric point on concrete as the "master". The master may have multiple degree of freedom (*dof*). The slave does not have its own *dof*, but can follow the movement of the master in a specified *dof*. Then, the "slave" is being connected to the "master" by introducing a single-point tying. In the MA case, only translation in x direction is allowed for both master and slave during tying to ensure that no CFRP end debonding occurs.

4.5 Creep Model

Creep test has been simulated based on the existing FE model for the MA slab. The creep model for concrete according to CEB-FIP Model Code 1990 has been adopted. The critical parameters for creep modeling are summarized in Table 4.8. In order to account the effect of prestressing in the strengthened slab, the FE model has been programmed to start the creep test simulation from the time of prestressing application by introducing a time curve in the analysis. Basically, the time curve depicts all the events throughout the time history during creep test analysis: firstly, the prestress has been applied at time 0; then, a sustained load of 20 kN has been applied to the slab 172 days after prestressing; and this sustained load has remained for 257 days until the load is removed at the end of the creep test. Since the total duration (about 257 days) of the analysis is considerably long, smaller time step is chosen only at the vicinity of loading and unloading in order to save computation time.

Table 4.8 Summary of creep model properties

Property	**Remarks**	**DIANA syntax**
Creep model	CEB-FIP Model Code 1990	CONCRE MC1990
Concrete grade	C30	GRADE C30
Young's modulus	30.4 GPa	YOUNG 3.04E+4
Ambient temperature	20 ºC	TEMPER 20
Relative humidity	50%	RH 50
Age at loading	250 days	LODAGE 250

CHAPTER 5 NUMERICAL SIMULATION RESULTS AND DISCUSSIONS

5.1 Numerical Simulation for Monotonic Load Tests

The numerical simulation results for the monotonic loading tests are compared with those obtained from experimental results. The following main aspects are compared: (i) load *vesus* mid-span displacement; (ii) load *vesus* mid-span concrete strains; (iii) load *vesus* mid-span CFRP strains; (iv) load *vesus* mid-span steel strains; and (v) crack patterns.

5.1.1 Load *vs* Mid-span Deflection

The comparisons between the experimental and numerical results of the applied load and mid-span deflection relationship for all slabs are shown in Figure 5.1 to 5.3. Generally, the curves depict three different stages of the slabs during loading, namely: (i) elastic phase — before crack initiation of concrete; (ii) cracked phase — from concrete cracking until yield initiation of steel reinforcement; and (iii) yielding phase — steel yielding until ultimate load failure. Similar trends are observed between the numerical and experimental results, capturing the key features during these stages for all slabs.

The numerical simulation gives accurate prediction of the deformation responses of three slabs in the elastic range before initiation of cracks occur in concrete. For the case of REF and EBR slabs, after concrete cracking, the numerical simulation still captures the key features of the deformation response such as steel yielding and ultimate failure, but with slight overestimation as compared to the experimental results. It is important to note that after cracks occur in concrete, the steel reinforcements (for REF) and CFRP (for EBR and MA) have become the main carrier of the applied load. The slight overestimation by numerical simulation may be due to the fact that during finite element modelling stage, a perfect bond has been assumed between the embedded steel reinforcements and concrete. In reality, there might be slip at steel-concrete interface and this has not been considered in the model. Additionally, the initial stress state due to the self-weight was not accounted for in the FE model.

It is interesting to note that for the case of MA slab, the numerical simulation precisely captures the intermediate debonding at about 55 kN with a horizontal curve shown in Figure 5.3. Since a linear elastic behavior is assumed for CFRP laminates, the ultimate load for MA slab in the numerical simulation is determined by the rupture of CFRP which has a tensile strength of 2375 MPa (see Chapter 3). The numerical simulation also captures the ultimate load with relatively good accuracy.

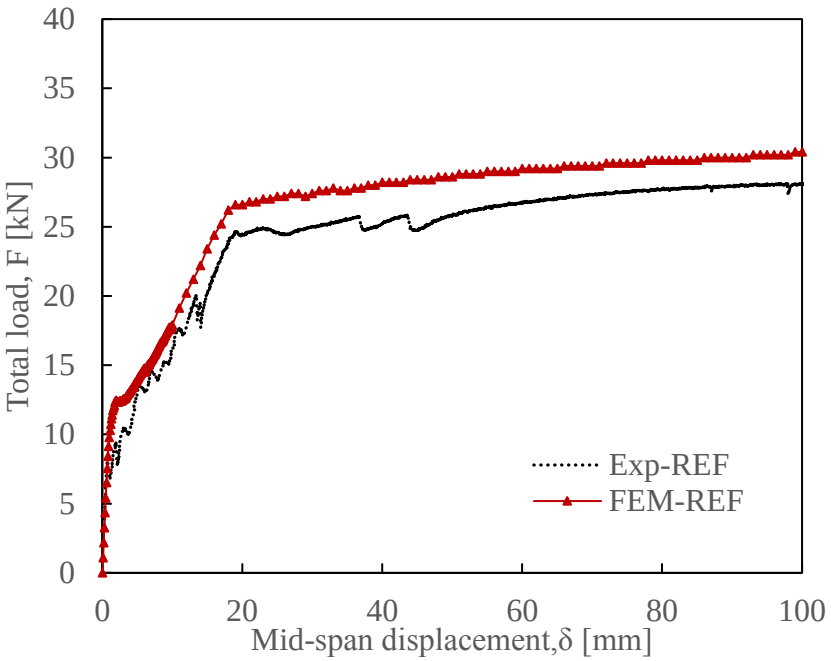

Figure 5.1 Load vs mid-span deflection graph comparison for REF slab

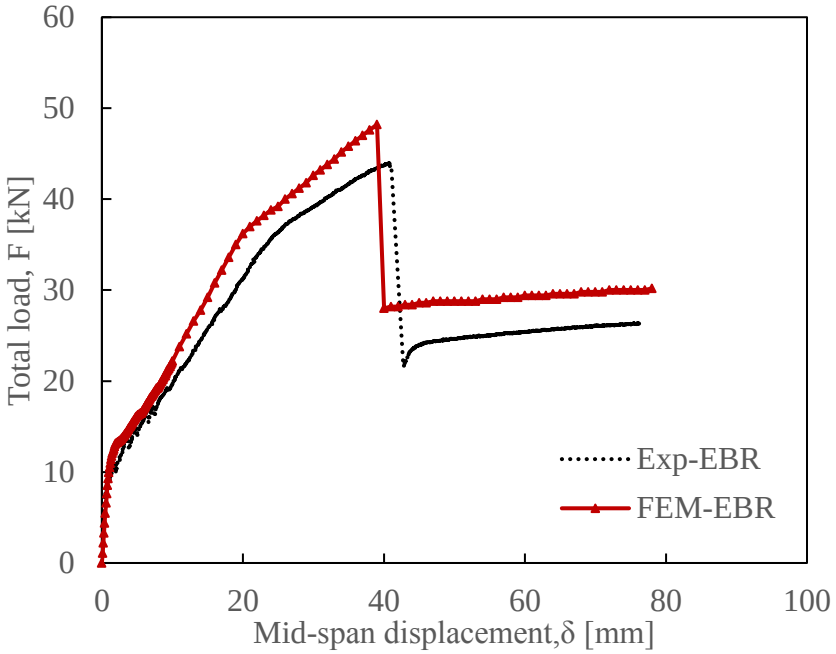

Figure 5.2 Load vs mid-span deflection graph comparison for EBR slab

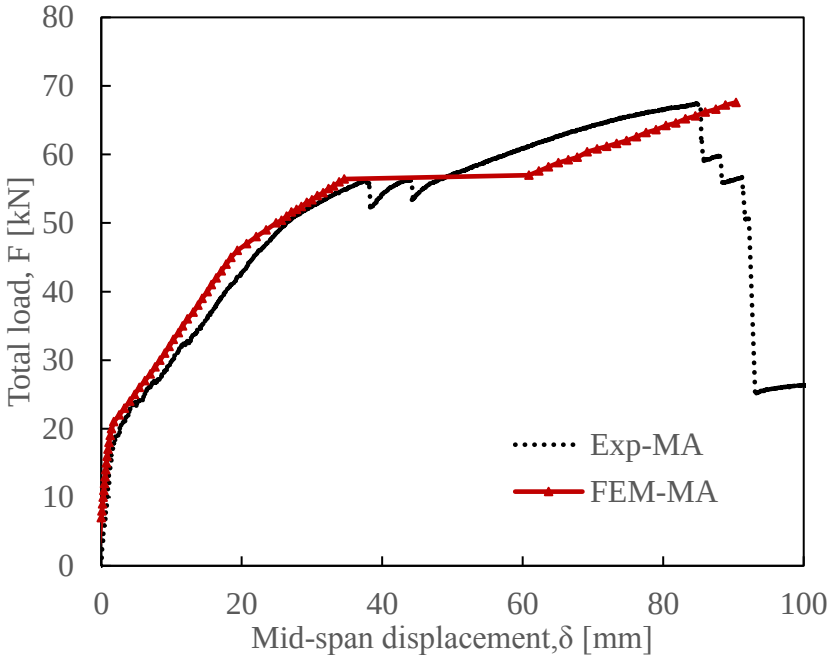

Figure 5.3 Load vs mid-span deflection graph comparison for MA slab

5.1.2 Load *vs* Mid-span Concrete Strain

The comparisons between the experimental and numerical results of the applied load and top mid-span top concrete strain relationship for all slabs are shown in Figure 5.4 to 5.6. The strain results are obtained for the concrete at the mid-span compression surface. The numerical and experimental results differ significantly, mainly in term of concrete strain values. This is due to the fact that, a linearly constant compression function has been adopted to describe the concrete behavior under compressive stress state. This compression function is usually for ideal case in which a constant softening law is used after the compressive strength of concrete is reached. It is worth pointing out that the numerical simulation agrees accurately with the experimental results in the elastic phase before crack initiation.

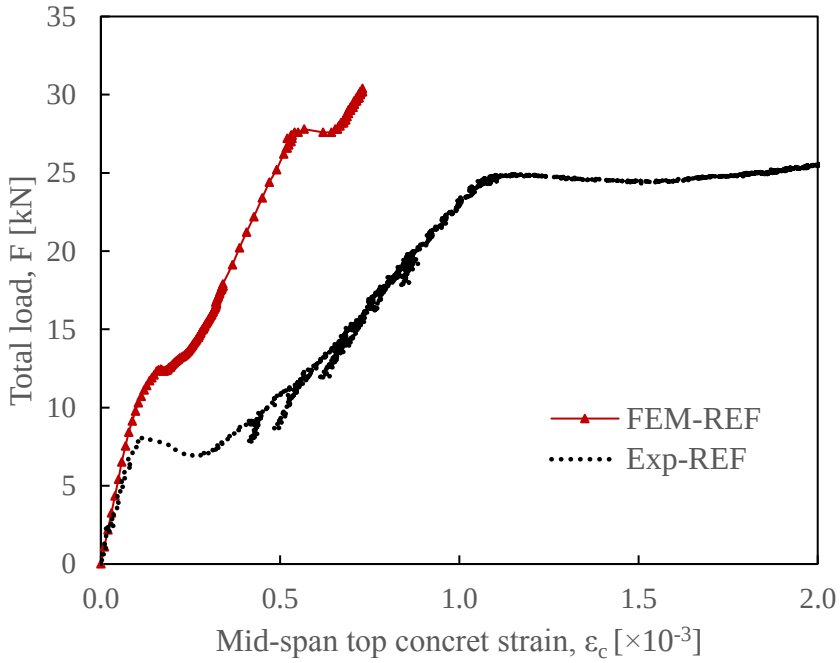

Figure 5.4 Load vs mid-span concrete strain graph comparison for REF slab

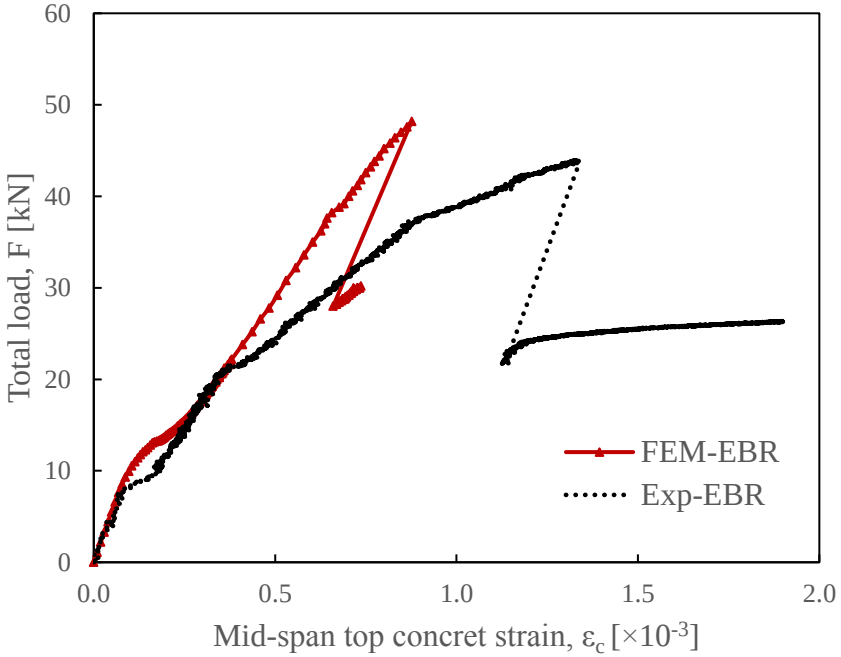

Figure 5.5 Load vs mid-span concrete strain graph comparison for EBR slab

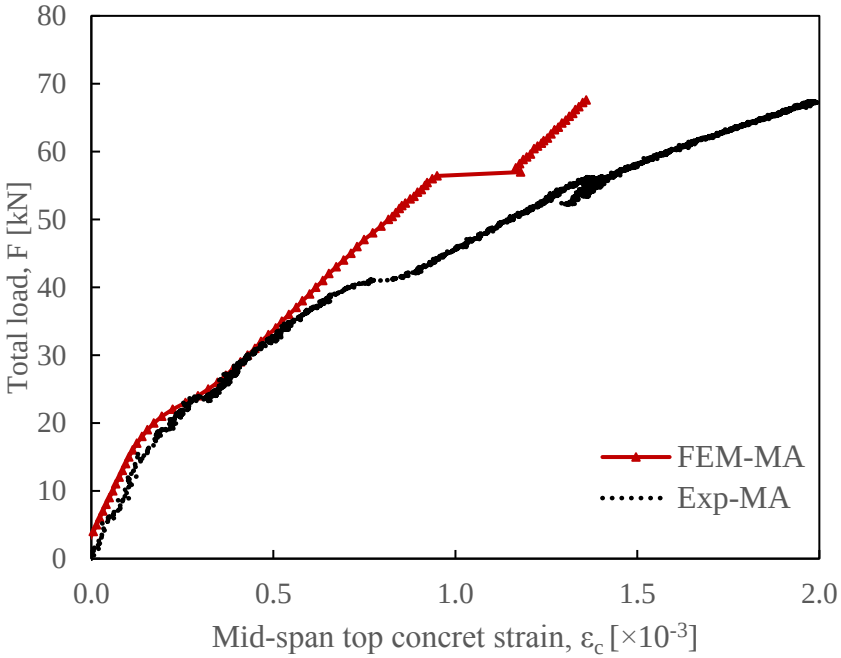

Figure 5.6 Load vs mid-span concrete strain graph comparison for MA slab

5.1.3 Load *vs* Mid-span CFRP Strain

The comparisons between the experimental and numerical results of the applied load and mid-span CFRP strain relationship for EBR and MA slabs are shown in Figure 5.7 and 5.8, respectively. Similar trend of load *versus* mid-span CFRP strain curves are observed between numerical and experimental results, with three distinct parts contributing to the overall curve (similar to that for load *versus* mid-span deflection curve): (i) before crack initiation of concrete; (ii) from concrete cracking until yield initiation of steel reinforcement; and (iii) from steel yielding until ultimate load failure.

Before concrete crack initiation, the strain change in CFRP laminates is minimal. The strain change in CFRP laminates becomes significant after concrete cracking occurs. Moreover, for the MA case, initiation of concrete cracking happens at a higher applied load of about 20 kN as compared to that of EBR slab at about 10 kN. This could be due to the contribution of the prestressed CFRP laminates as well as fixed mechanical anchorage system.

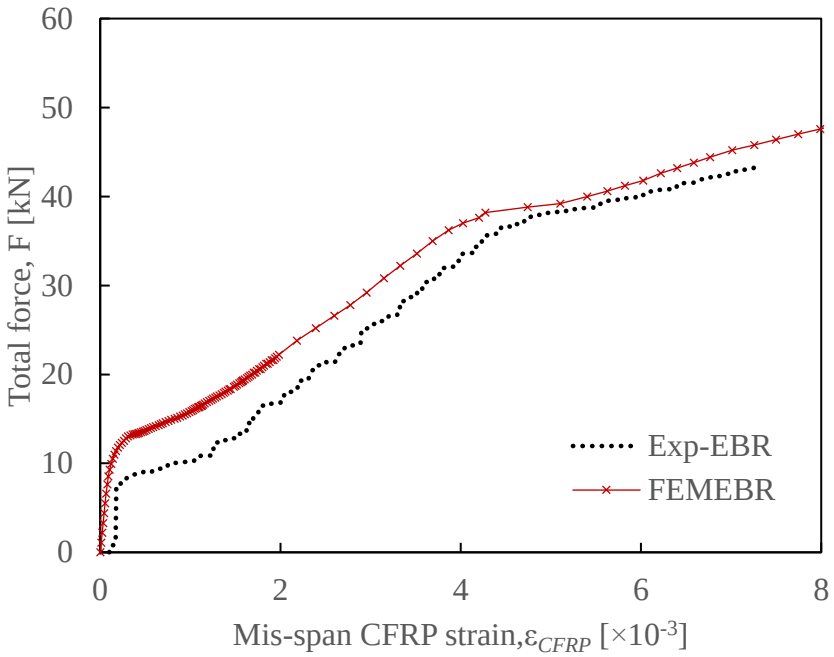

Figure 5.7 Load vs mid-span CFRP strain graph comparison for EBR slab

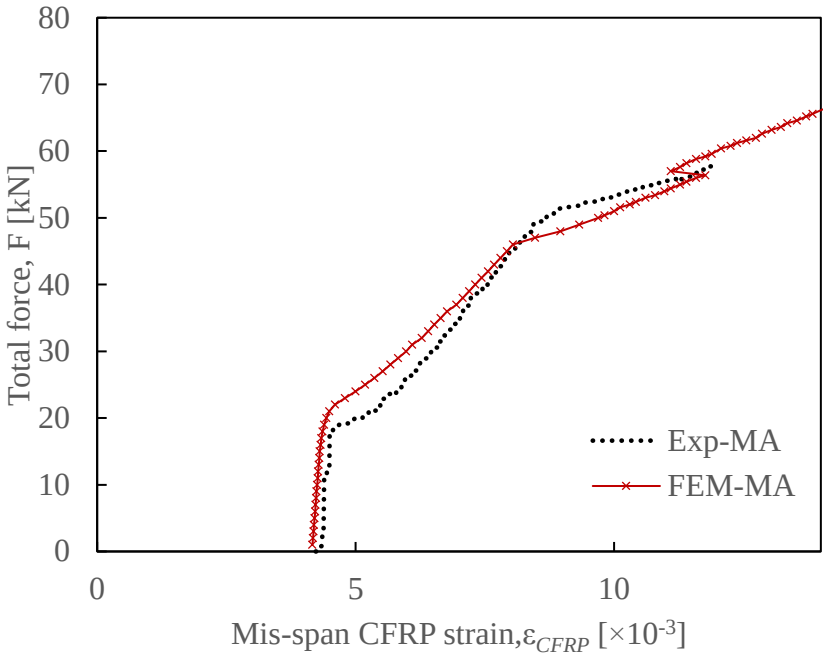

Figure 5.8 Load vs mid-span CFRP strain graph comparison for MA slab

5.1.4 Load *vs* Mid-span Longitudinal Steel Strain

It is important to monitor the strain evolution with the applied load for steel reinforcement in tension. However, the strain of the bottom longitudinal steel reinforcement (ϕ8) was not measured during the experiment due to the difficulty of implementation. The numerical results of the applied load and mid-span bottom longitudinal steel reinforcement strain relationship for all slabs are shown in Figure 5.9. The yield strain ε_y of the steel reinforcement is approximately 2.5 ‰ and this value corresponds to a yield strength of 500 MPa which is close to the yield strength of the steel reinforcement used in the model after the modification of reduced yield envelope (520 MPa). As such, the bottom steel reinforcement has reached yielding point. Therefore, as expected, it can be easily seen that the strengthened RC slabs (EBR and MA) reach higher loads when the steel reinforcement has yielded. Moreover, similar strain response is observed for EBR and MA, with MA sustaining higher load than EBR for the same strain level.

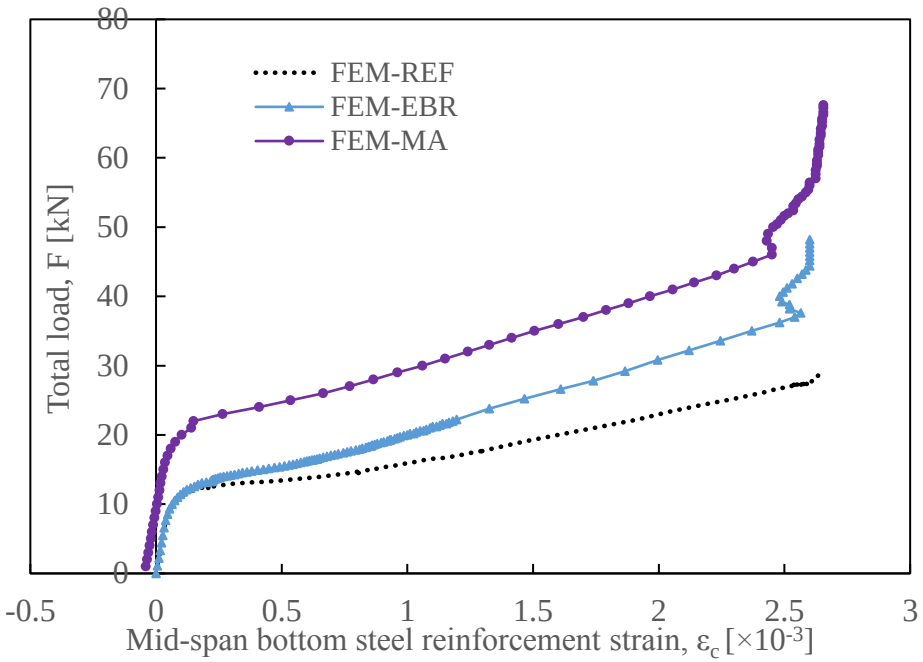

Figure 5.9 Load vs mid-span steel strain graph from numerical simulations

5.1.5 Crack Patterns

The crack pattern of the tested slabs were monitored and recorded for the whole span length as shown in Figure 5.10. The crack patterns from the final step of the numerical simulations are illustrated in Figure 5.11 to 5.13 which only shows half span of the slabs. By comparison, it can be concluded that the numerical simulation is able to predict the crack patterns with relatively high accuracy. Generally, both experimental and numerical results show that cracks locate at the tensile surface of the slabs near the proximity of the loading point.

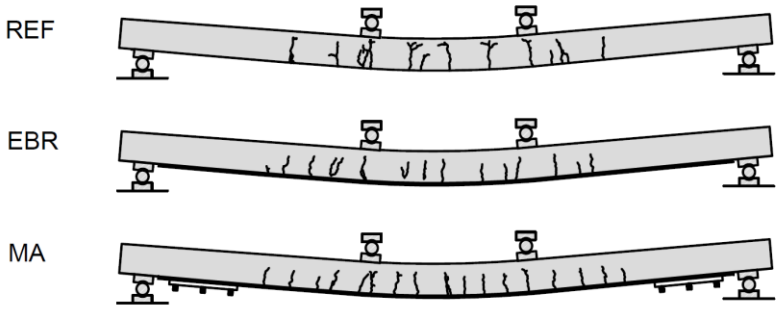

Figure 5.10 Crack patterns of all slabs from experimental results

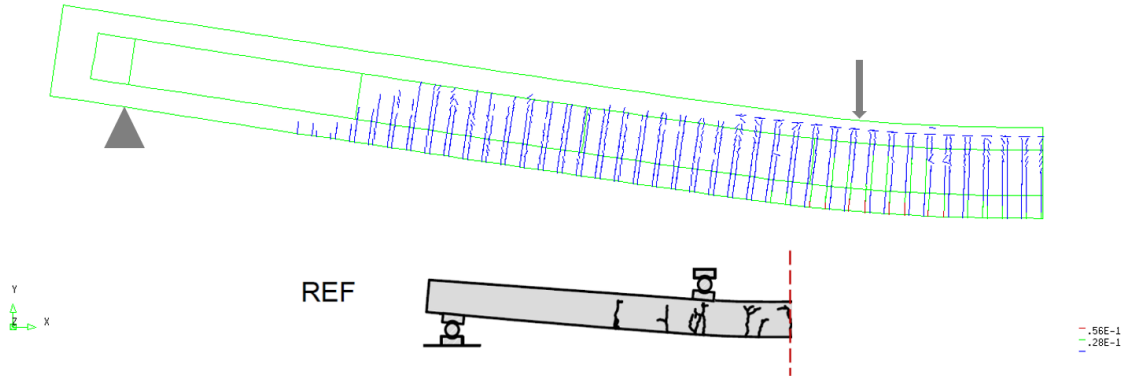

Figure 5.11 Crack patterns from numerical simulation-REF slab

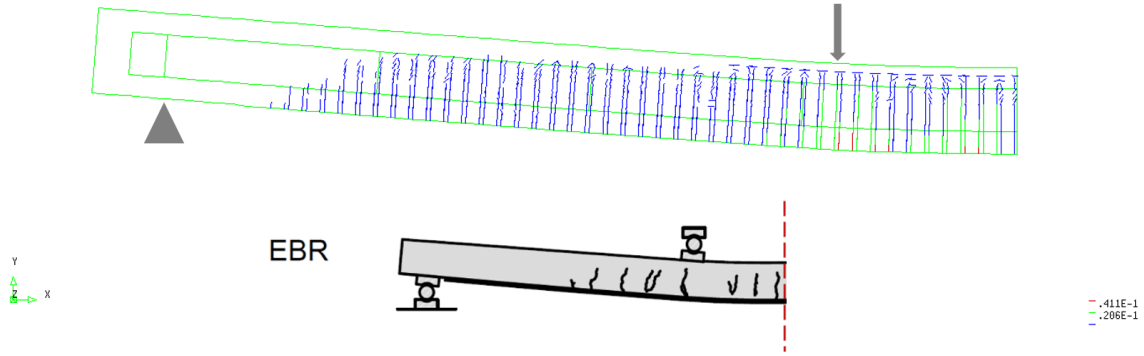

Figure 5.12 Crack patterns from numerical simulation-EBR slab

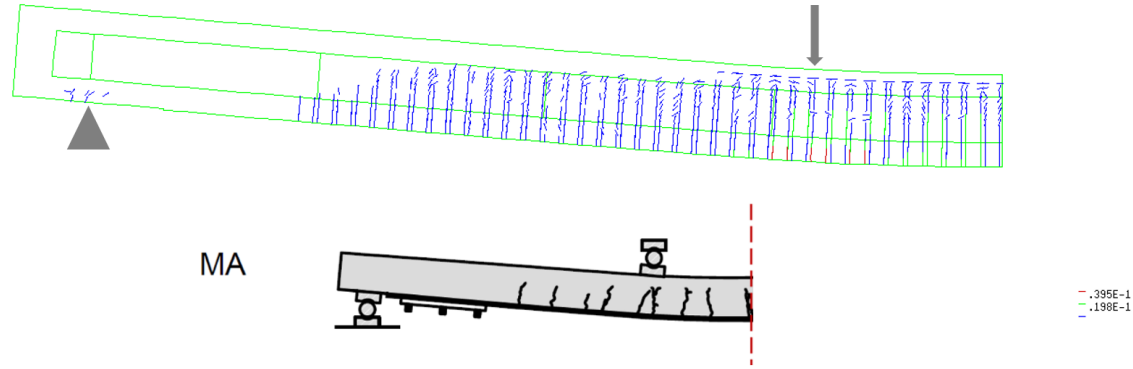

Figure 5.13 Crack patterns from numerical simulation-MA slab

5.2 Numerical Simulation for Creep Test

The numerical simulation results of time evolution of mid-span deflection of the MA slab for creep test are compared with the experimental results. Factors affecting the creep test

are briefly discussed. Important simulation results such as prestress loss in CFRP laminate is also presented.

5.2.1 Effects of Temperature and Relative Humidity

The comparison of time evolution of mid-span deflection of the MA slab between the experimental and numerical results is presented in Figure 5.14. The FE model provides the overall results with high accuracy for the long-term behavior of the MA slab during creep test. However, it should be noted that there is a distinct overestimation for mid-span deflection by the FE model before time reaches 75 days. In the actual experiment, the slab was only submitted to the controlled environment (20 ºC and 50% RH) after 350 hours from the beginning of the creep test. In addition, the creep test was carried out from 17-Dec-2014 onwards, which was the winter season where the RH and the average ambient temperature were much lower than the controlled environment (20ºC and 50% RH). Furthermore, for the first 350 hours, the slab was subjected to laboratory environment which the daily temperature usually vary more than 10 ºC. These factors have not been considered in the numerical simulation. In the FE model, a constant temperature of 20ºC and 50% RH is assumed in the simulation. Since creep increases with increasing temperature [Bazant and Wittmann, 1982], this might be a possible explanation for the distinct difference at the early stage of the creep test.

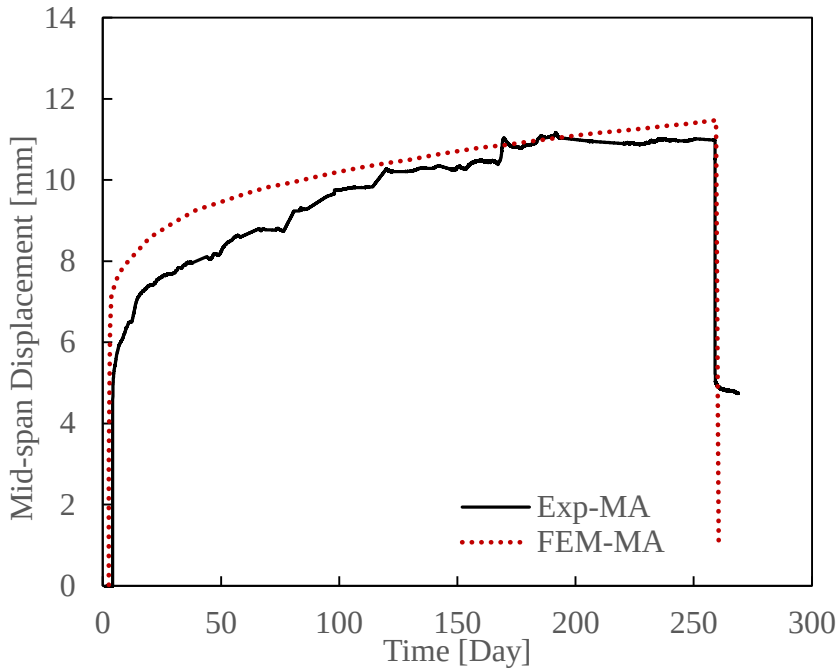

Figure 5.14 Time evolution of mid-span deflection comparison for creep test

5.2.2 Loss of Prestress in CFRP

Since the FE model starts the creep modelling from the day of prestressing application, it is important to check the prestress loss till the day of creep test. As such, the numerical results of time evolution of mid-span CFRP stress from the day of pretressing application till the day of creep test which is a total period of 172 days is presented in Figure 5.15. The initial applied prestress is 680 MPa, and the prestress gradually decreases to 650 MPa over 172 days. This prestress loss corresponds to approximately 4% which is relatively negligible. Therefore, the loss of prestress in CFRP laminate of the present strengthened RC slab is minimal.

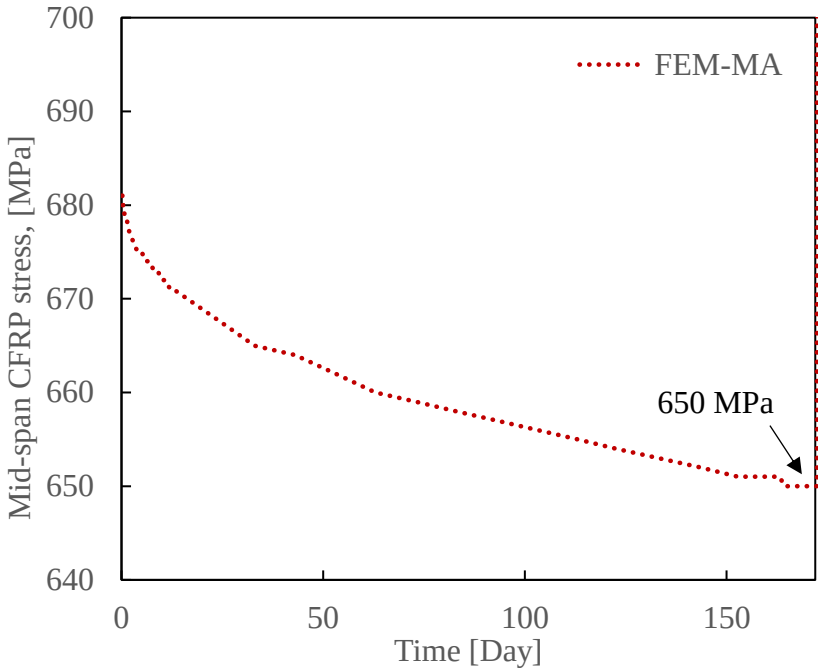

Figure 5.15 Time evolution of mid-span CFRP stress prior to creep test

5.3 Conclusions

In summary, the numerical simulation predicts the structural behaviors of the RC slabs accurately, capturing the critical stages such as crack initiation, yielding and ultimate failure with relatively high precision. A summary of these important parameters is presented in Table 5.1. Good agreement has been established between the experimental and numerical results. In addition, the creep model developed based on existing FE model also correlates very well with the experimental results, making the numerical simulation as a reliable tool to predict the long-term behaviors of the CFRP strengthened RC slabs.

Table 5.1 Main summary of numerical simulation results

	Stiffness		**Crack Initiation**		**Yielding**		**Ultimate**	
	K_I [kN/mm]	K_{II} [kN/mm]	δ_{cr} [mm]	F_{cr} [kN]	δ_y [mm]	F_y [kN]	δ_{max} [mm]	F_{max} [kN]
REF	11.71	0.52	1.11	13	18	26.2	100	30.2
EBR	9.17	1.34	1.2	11	20	36.2	39	48.2
MA	11.80	1.42	1.78	21	19.4	46	90.4	67.6

CHAPTER 6 PARAMETRIC STUDIES

6.1 Introduction

A series of parametric studies have been developed to investigate the influence of important parameters defining the prestressed slab's characteristics. A controlled slab is used as the reference slab (REF-P) with its properties shown in Table 6.1. Since it has been proven from the experimental results that the RC slab strengthened with CFRP laminate by MA shows excellent performance in terms of overall structural behavior, the parametric studies is developed based on the MA method. The objective of the parametric studies is to evaluate the sensitivity of the REF-P slab with variations of the following three parameters: (i) prestress level; (ii) concrete grade; and (iii) CFRP laminate geometry. For each group, two parameter variations will be compared with that of REF-P. As such, prestress level at 0.6% and 0.8%, concrete grade of C35/45 and C40/50, and CFRP laminate geometry of 80 × 1.2 and 100 × 1.2 will be studied. The CFRP laminate has the same Young's modulus of elasticity and ultimate tensile strength regardless of geometry.

Table 6.1 Summary of parameter variations for parametric studies

	Prestress	**Concrete grade**	**CFRP geometry**
REF-P	0.4%	C30/37	50 × 1.2
PR-0.6%	0.6%	C30/37	50 × 1.2
PR-0.8%	0.8%	C30/37	50 × 1.2
CG-C35/45	0.4%	C35/45	50 × 1.2
CG-C40/50	0.4%	C40/50	50 × 1.2
LG-80× 1.2	0.4%	C30/37	80× 1.2
LG-100× 1.2	0.4%	C30/37	100× 1.2

Note: C35/45 (f_{cm}=43 MPa, E_c=34 GPa); C40/50 (f_{cm}=48 MPa, E_c=35 GPa)
CFRP: E=170 GPa, f_u=2500 MPa

6.2 Variation in Prestress Level

The comparison of load *versus* mid-span displacement for CFRP laminate with various prestress level is illustrated in Figure 6.1. It is obvious that the prestress levels of CFRP laminate significantly contribute to the load-displacement responses. A higher prestress level yields a lower mid-span deflection at ultimate load, reducing the ductility of the slab. However, the

effects of increasing prestress levels in CFRP laminate on the mid-span deflection at cracking and yielding are not as significant as those on the ultimate loads. This phenomenon is due to the fact that the total CFRP strains are fixed and thus the usable CFRP strains are decreased when the initial prestress level is increased. Moreover, an increase of cracking and yielding loads is observed with increasing prestress level in CFRP laminate. On the other hand, the ultimate loads for the three slabs with different prestress levels are approximately the same, implying that the prestress level does not contribute to the enhancement of the ultimate load capacity of the strengthened slabs. This behavior is within the expectation since the failure of the slab occurred by the tensile rupture of the CFRP laminate.

Figure 6.2 and 6.3 show the strain development for CFRP, concrete and steel at mid-span with various prestress levels of CFRP laminate, respectively. There is no significant strain changes in the prestressed CFRP laminate (Figure 6.2) and steel reinforcement (Figure 6.3) until cracking. However, the influence of CFRP prestress levels on strain increment has become considerably remarkable after cracking, and such influence becomes especially obvious after yielding. As expected, as the applied load increases, the CFRP strains converge to approximately the same ultimate strain value for different prestress levels. This phenomenon provides an explanation for the similar ultimate failure loads observed in Figure 6.1. In summary, an increase in prestress level of CFRP laminate contributes to a greater load capacity at cracking and yielding, however, it does not affect the ultimate load capacity. Furthermore, a higher prestress level in CFRP laminate yields a lower ultimate mid-span deflection and consequently reduces the ductility, but has minimal effect on the deflection at cracking and yielding.

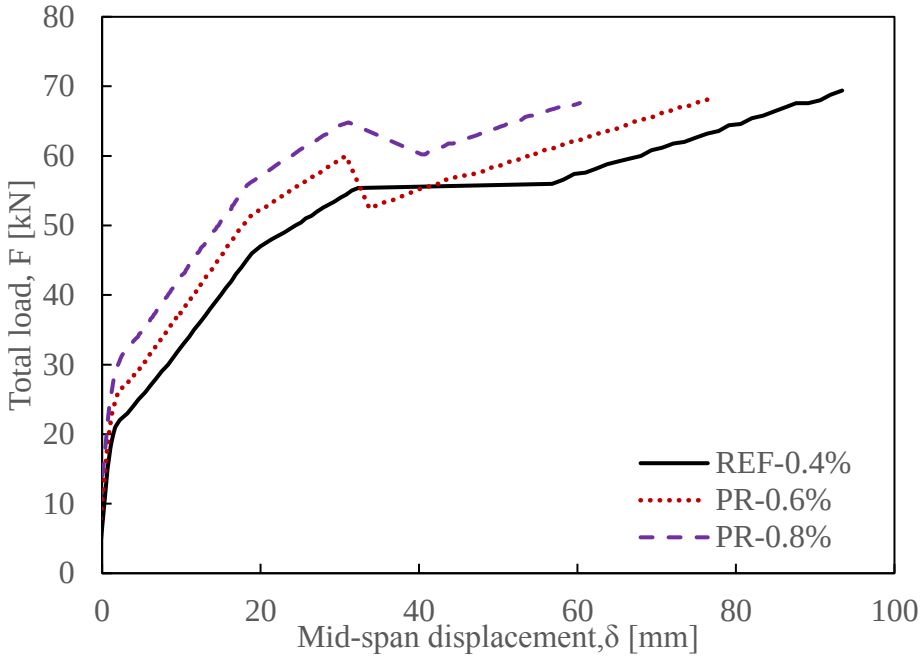

Figure 6.1 Load vs mid-span deflection graph comparison for variation of prestress levels

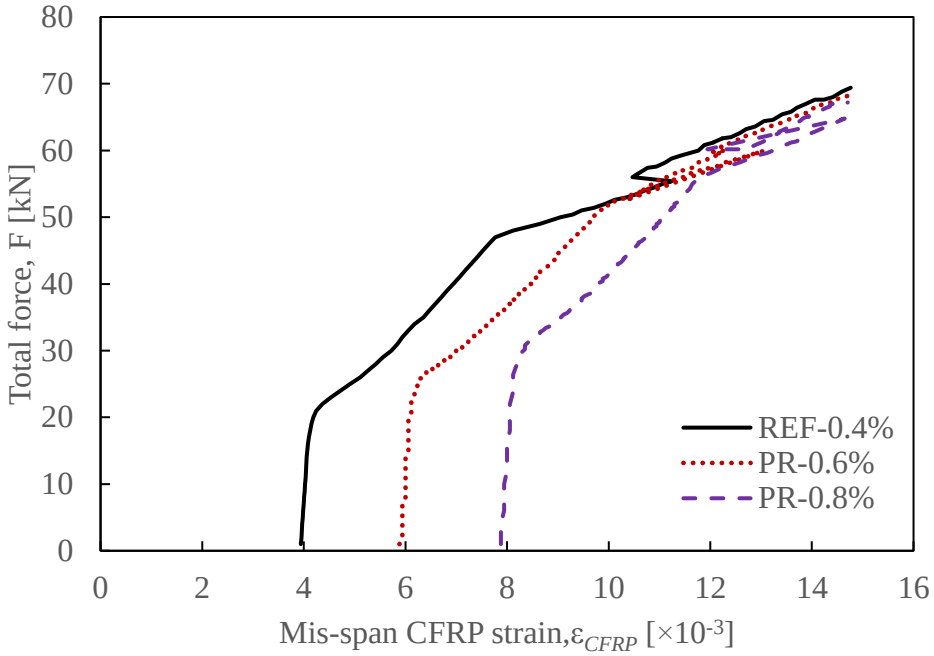

Figure 6.2 Load vs mid-span CFRP strain graph comparison for variation of prestress levels

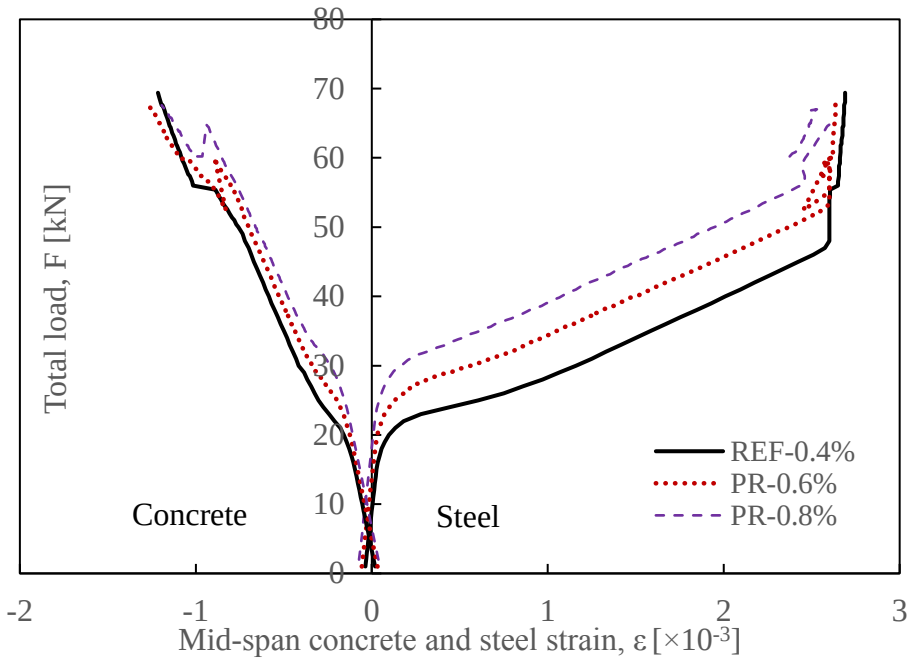

Figure 6.3 Load vs mid-span concrete and steel strain graph comparison for variation of prestress levels

6.3 Variation in Concrete Grade

The comparison of load *versus* mid-span displacement for CFRP strengthened slabs with various concrete grades is illustrated in Figure 6.4. Figure 6.5 and 6.6 shows the strain development for CFRP, concrete and steel at mid-span with various concrete grades, respectively. Similar trend in load-deflection response is observed for the slabs with three different concrete grades, except for the distinct intermediate debonding behaviors. The strain development for CFRP and steel at mid-span is not affected significantly by variation of concrete grades as shown by Figure 6.5 and 6.6. Therefore, it can be concluded that by changing the concrete grades from C30/37 to C35/45 and C40/50, the enhancement in load capacity at cracking, yielding and ultimate failure is not significantly affected. It should be stressed that the variation of concrete grade mainly affected the tensile response of this material since under compression, in all the simulations a linear elastic behavior was assumed. This assumption was adopted since in the experiments crushing of the concrete under compressive forces was never experienced.

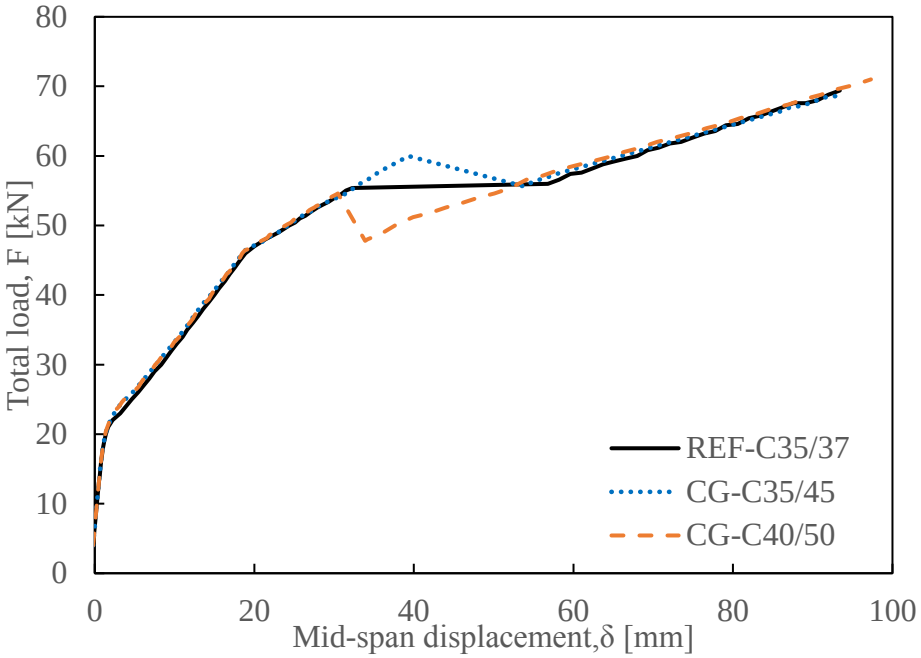

Figure 6.4 Load vs mid-span deflection graph comparison for variation of concrete grade

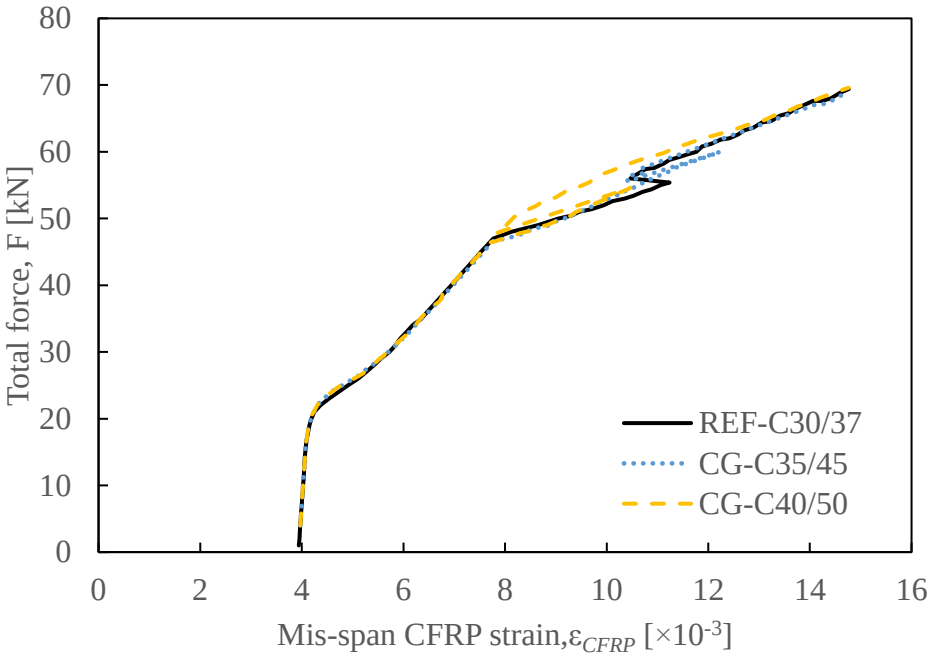

Figure 6.5 Load vs mid-span CFRP strain graph comparison for variation of concrete grade

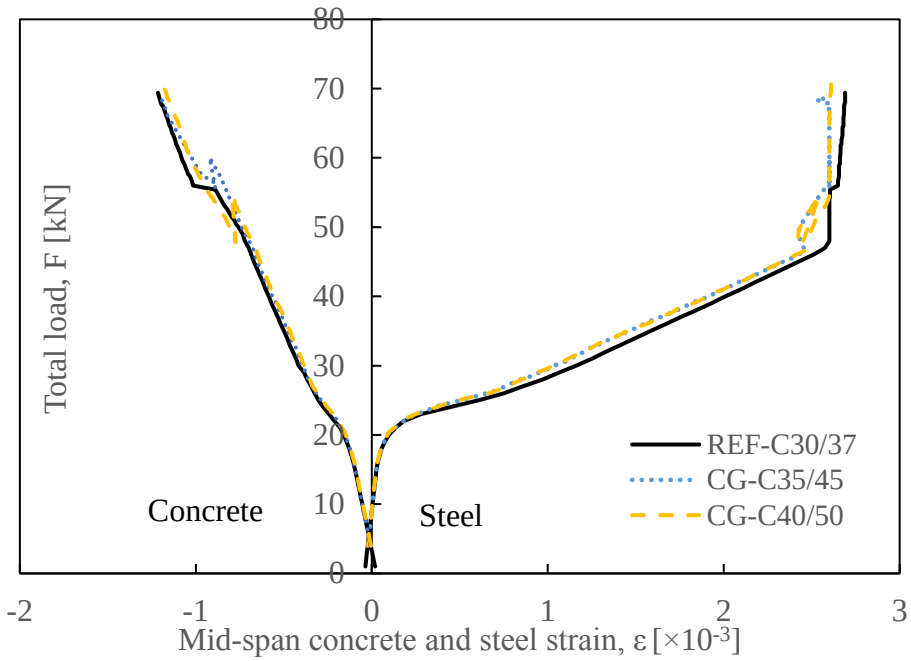

Figure 6.6 Load vs mid-span concrete and steel strain graph comparison for variation of concrete grade

6.4 Variation in CFRP Laminate Geometry

The comparison of load *versus* mid-span displacement for CFRP strengthened slabs with various CFRP laminate geometry is illustrated in Figure 6.7. Figure 6.8 and 6.9 shows the strain development for CFRP, concrete and steel at mid-span of the slabs with various CFRP laminate geometry, respectively. It clearly demonstrates the significance of the CFRP laminate geometry on the load-deflection (Figure 6.7). Generally, a larger cross-sectional area of the CFRP laminate contributes to a greater load capacity at all critical stages, being cracking, yielding and ultimate failure. This benefit is especially obvious at ultimate failure with approximately 38% and 63% increase in ultimate load capacity for LG-80×1.2 and LG-100×1.2, respectively, as compared to REF-50×1.2. As shown in Figure 6.8, the slabs strengthened with different CFRP laminate geometry reach the same ultimate CFRP strain, however, slabs strengthened with larger cross-sectional CFRP laminate area bear higher ultimate failure load. Therefore, it can be concluded that a larger cross-sectional area of CFRP laminate contributes to an increase in load capacity at cracking, yielding and especially ultimate failure.

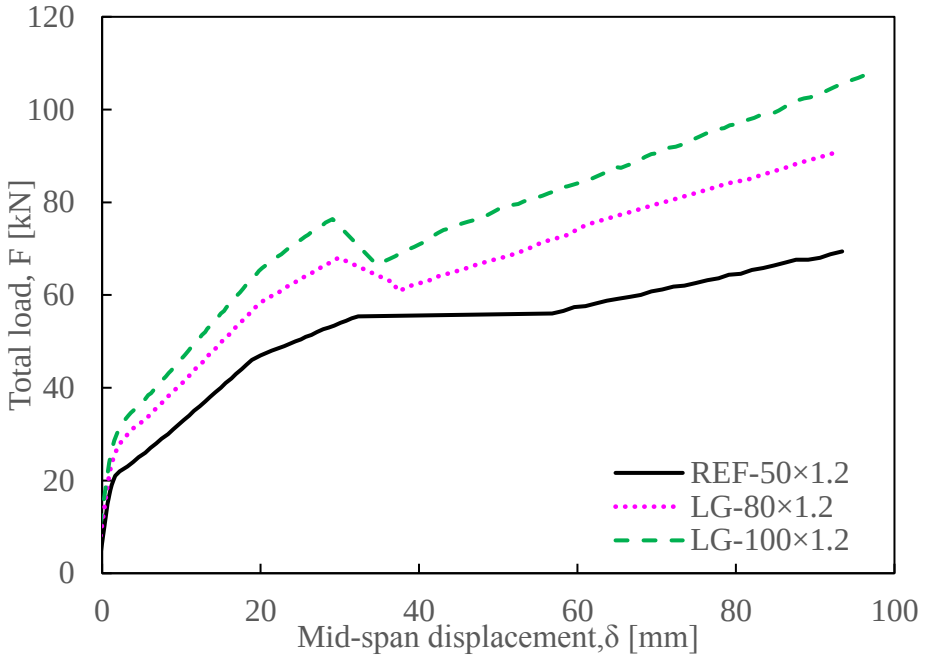

Figure 6.7 Load vs mid-span deflection graph comparison for variation of CFRP geometry

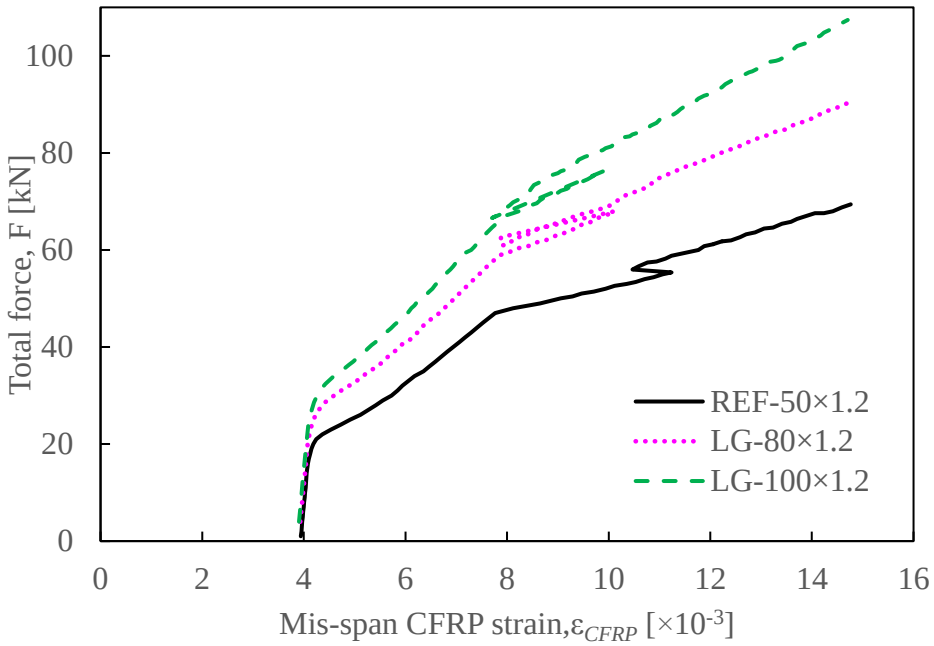

Figure 6.8 Load vs mid-span CFRP strain graph comparison for variation of CFRP geometry

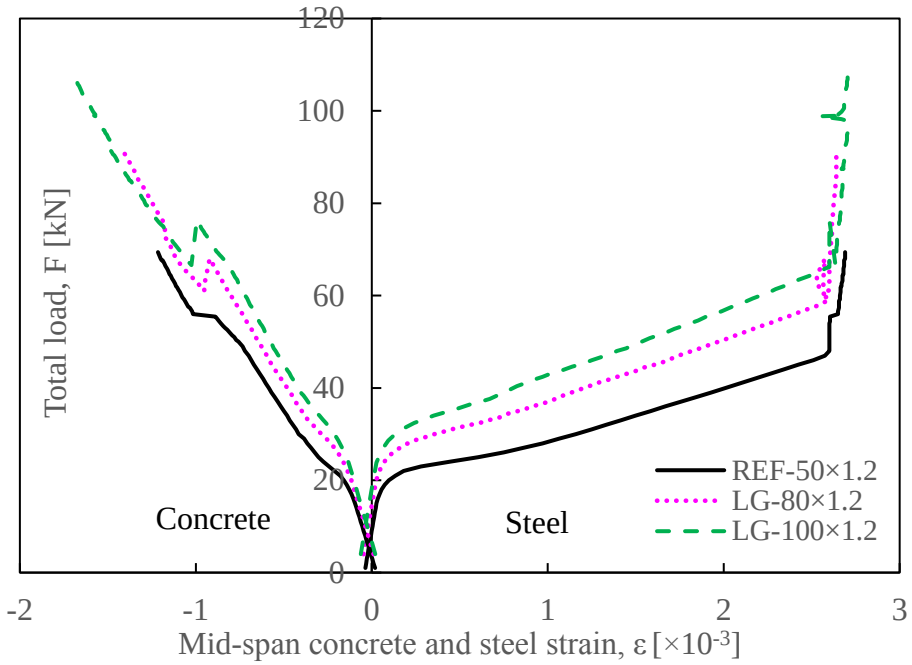

Figure 6.9 Load vs mid-span concrete and steel strain graph comparison for variation of CFRP geometry

6.5 Summary

The important simulation results from parametric studies are summarized in Table 6.2 below. Figure 6.10 and 6.11 further illustrates the effects of variation of different parameters on total applied load and mid-span deflection, respectively. Critical aspects such as crack initiation, yielding and ultimate failure are depicted. Moreover, the stiffness at elastic uncracked phase (K_I) and after cracking (K_{II}) are also compared in Figure 6.12. The influence of variation of different parameters on K_I is significant whereas after cracking occurs, the stiffness (K_{II}) becomes unaffected by such variations. The following conclusions can be made from parametric studies:

(i) **Prestress level of CFRP laminate**: an increase in prestress level from 0.4% to 0.6% and 0.8% respectively provides significant enhancement of load capacity at crack initiation and yielding, but not at ultimate failure load. On the other hand, the increase in prestress level does not affect the mid-span deflection at crack initiation and yielding, whereas it results in a significant reduction in mid-span deflection at ultimate failure. In

addition, the stiffness at elastic phase (K_I) is increased with higher prestress level of CFRP laminate.

(ii) **Concrete grade**: an increase of concrete grade (and thus the compressive strength and modulus of elasticity) from C30/37 to C35/45 and C40/50 respectively provides minimal enhancement in terms of load capacity and mid-span deflection. A marginal increment of K_I is observed with an increase in concrete grades.

(iii) **CFRP laminate geometry**: an increase of CFRP laminate cross-sectional area from 50 × 1.2 to 80 × 1.2 and 100× 1.2 respectively results in a significant increment of load capacity at crack initiation and yielding, and such enhancement becomes considerably remarkable at ultimate failure. On the other hand, the mid-span deflection at all critical stages (crack initiation, yielding and ultimate failure) is not affected by the variation of laminate geometry. Furthermore, the increase in K_I is significant with larger cross-sectional area of CFRP laminate.

Table 6.2 Main summary of results from parametric studies

	Stiffness		**Crack Initiation**		**Yielding**		**Ultimate**	
	K_I [kN/mm]	K_{II} [kN/mm]	δ_{cr} [mm]	F_{cr} [kN]	δ_y [mm]	F_y [kN]	δ_{max} [mm]	F_{max} [kN]
REF-P	9.87	1.41	2.23	22.0	33.7	52.6	93.4	69.4
PR-0.6%	14.08	1.53	1.79	25.2	30.8	60.0	76.6	68.2
PR-0.8%	15.44	1.54	1.93	29.8	30.5	64.6	60.3	67.6
CG-C35/45	10.67	1.43	2.10	22.4	39.3	60.0	92.9	68.6
CG-C40/50	10.98	1.43	2.04	22.4	30.5	54.6	97.3	71.0
LG-80x1.2	14.75	1.75	1.79	26.4	29.9	68.0	92.7	90.8
LG-100x1.2	15.89	1.95	1.90	30.2	28.2	75.6	97.7	108.0

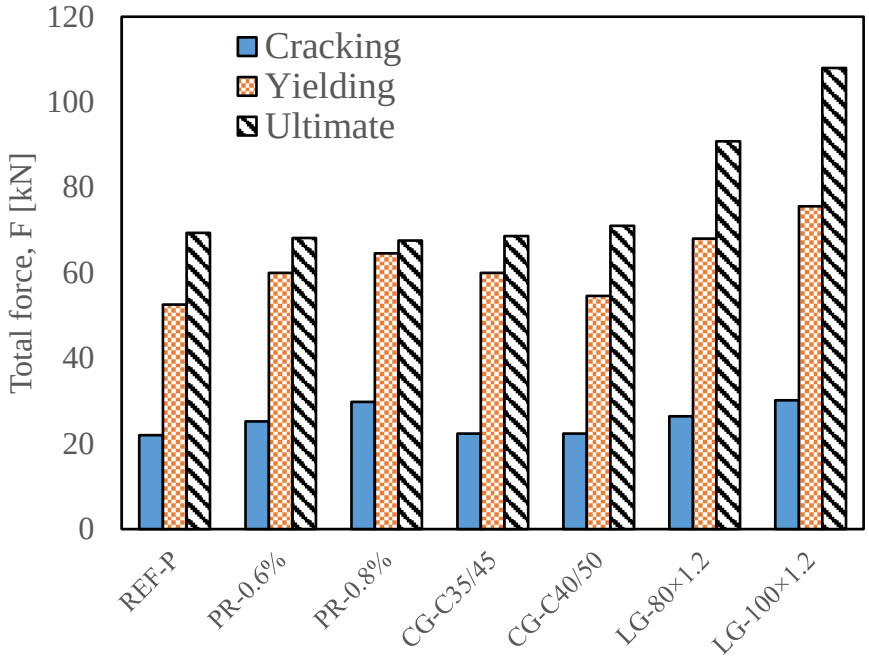

Figure 6.10 Load variation for slabs from parametric studies

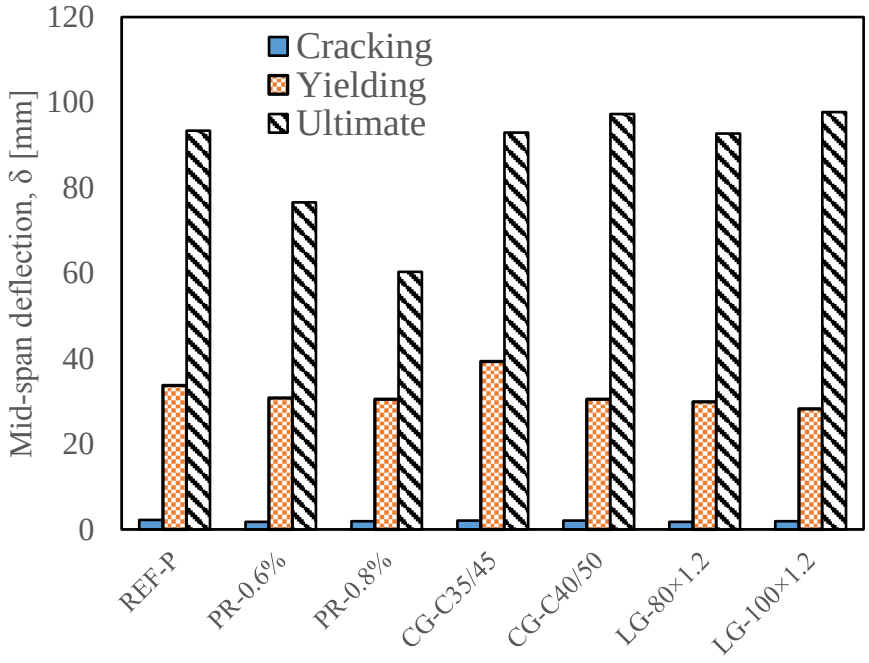

Figure 6.11 Mid-span deflection variation for slabs from parametric studies

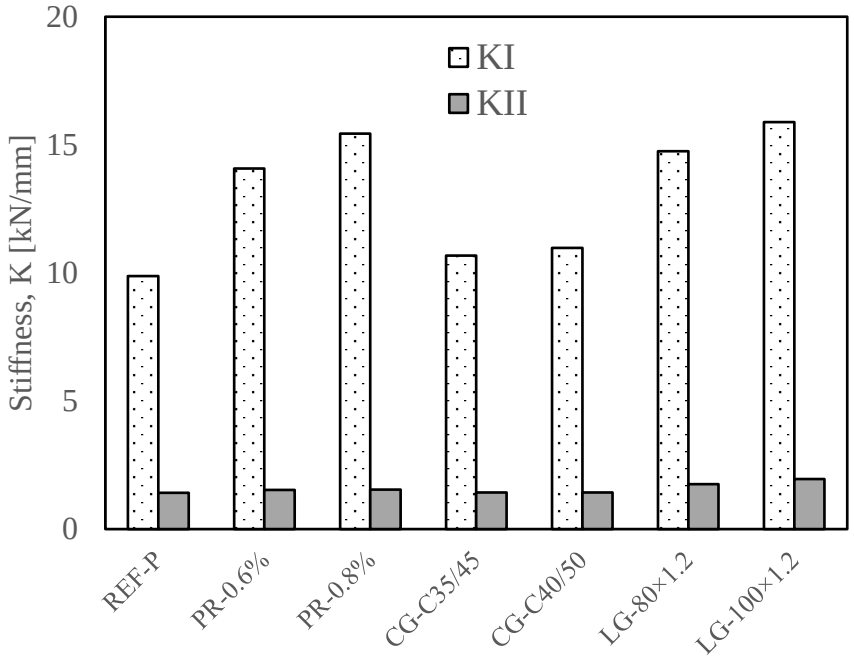

Figure 6.12 Stiffness variation for slabs from parametric studies

CHAPTER 7 CONCLUSIONS AND RECOMMENDATIONS

7.1 Conclusions from Present Study

The objectives of this study has been achieved. FE models have been developed to simulate numerically the experimental results of the prestressed slabs tested up to the failure and under sustained loads (creep test). By comparisons of the relevant results, good correlations have been found between the numerical and experimental results. Since the existing FE models predict the structural behavior of the slabs with high accuracy, parametric studies have been performed based on these models to analyse the effect of relevant variables, such as prestressing level, concrete grade and CFRP laminate geometry.

Several conclusions can be drawn from this study. The performance of RC slabs strengthened with CFRP (both prestressed and non-prestressed) are significantly improved in terms of lower deflection, crack width delay and lower crack spacing. In addition, the metallic anchors composing the MA system prevented a premature failure by debonding and allowed the slabs to support higher ultimate loads and deflections. A greater use of the CFRP laminate strip tensile capacity was attained when prestressing was applied to the CFRP laminates. The average ultimate strain on the CFRP laminate increased by 74% with prestressing for the slabs tested. Furthermore, the initial loss of prestress in CFRP laminate is relatively negligible, making it a promising strengthening material.

From parametric studies, several conclusions can be summarized based on this study. An increase in prestress level provides significant enhancement of load capacity at crack initiation and yielding, and a significant reduction in mid-span deflection at ultimate failure. The variation of concrete grade results minimal enhancement in terms of load capacity and mid-span deflection. By increasing the cross-sectional area of CFRP laminate, the load capacity at crack initiation and yielding is significantly increased, and such enhancement becomes considerably remarkable at ultimate failure.

7.2 Recommendations for Future Work

Based on this study, several recommendations are suggested for future work in the area of structural behaviors of RC slabs strengthened with prestressed CFRP laminates. The long-term behavior of the strengthened slabs can be further explored in depth. From this study, it has been concluded that the existing FE model provides an accurate simulation as the experimental creep tests. Future work in the area of FEM simulation of long-term behavior of the strengthened slabs, taking into account the temperature influence can be developed. In addition, the viscoelastic effects of prestressed CFRP can also be explored thoroughly. Furthermore, the durability of the strengthened slabs when subjected to extreme temperatures or harsh environment is also an interesting research area.

REFERENCES

1. Aram MR, Czaderski C, Motavalli M. (2008). "Effects of gradually anchored prestressed CFRP strips bonded on prestressed concrete beams". *Journal of Composites for Construction 12(1):25-34.*
2. Barros J., Ferreria D., Fortes A., Dias S. (2006). "Assessing the effectiveness of embedding CFRP laminates in the near surface for structural strengthening". *Construction and Building Materials 20(7): 478-491.*
3. Bazant Z., Wittmann F. (1982). "Creep and Shrinkage in Concrete Structures". *John Wiley & Sons, New York, US.*
4. Bilotta A, Ceroni F, Nigro E, Pecce M. (2015). "Efficiency of CFRP NSM strips and EBR plates for flexural strengthening of RC beams and loading pattern influence". *Composite Structures 124: 163-175.*
5. Blaschko, M., and Zilch, K. (1999). "Rehabilitation of concrete structures with CFRP strips glued into slits." *Proceedings of the 12th International Conference on Composite Materials*, Paris, France.
6. CEB-FIP Model Code for Concrete Structures (1990). *Published by Thomas Telford Services Ltd, Thomas Telford House, 1993.*
7. Chen JF, Teng JG. (2001). "Anchorage strength models for FRP and steel plates bonded to concrete". *Journal of Structural Engineering, ASCE 127(7):784–91.*
8. Correia, L.; Teixeira, T.; Michels, J.; Almeida, J.; Sena-Cruz, J. (2015). "Flexural behaviour of RC slabs strengthened with prestressed CFRP strips using different anchorage systems." *Composites Part B, (81): 158–170.*
9. de Borst, R., and Nauta, P. (1985). "Non-orthogonal cracks in smeared finite element model." *Engineering Computations Journal, (2): 35-46.*
10. DIANA-9.6 User's Manual. (2015). "DIANA Finite Element Analysis Release Notes 9.6". *Copyright by TNO DIANA.*
11. El-Hacha, R., Wight, R. G., & Green, M. F. (2001). "Prestressed fibre-reinforced polymer laminates for strenghtening structures". *Progress in Structural Engineering and Materials (3): 111–121.*

12. Fernandes P, Granja J, Benedetti A, Sena-Cruz J, Azenha M. (2015). "Quality control and monitoring of NSM CFRP systems: E-modulus evolution of epoxy adhesive and its relation to the pull-out force". *Composites Part B (75):95-103.*

13. Godat A., Labossière P., Neale K. (2010). "Numerical Modeling of the FRP/Concrete Interfacial Behavior of FRP Shear-Strengthened Beams". *The 5th International Conference on FRP Composites in Civil Engineering September 27-29, 2010 Beijing, China.*

14. Hordijk D., Reinhardt H., Cornelissen H. (1987). "Fracture mechanics parameters of concrete from uniaxial tests as influenced by specimen length". *Proceedings SEM-RELIM Internaltional Conference on Fracture of Concrete and Rock, 138-149.*

15. ISO 527-5. (1997). "Plastics d Determination of tensile properties d Part 5: test conditions for unidirectional fibre-reinforced plastic composites". Genève: ISO-International Organization for Standardization.

16. LNEC E397-1993. (1993). "Concrete e determination of the elasticity young modulus under compression" [Portuguese specification from LNEC].

17. Lorenzis, L. De., Miller, B., and Nanni, A. (2001). "Bond of Fiber-Reinforced Polymer Laminates to Concrete". *ACI Material Journal, 98(3): 256-264.*

18. Michels J, Sena-Cruz J, Czaderski C, Motavalli M. (2013). "Structural strengthening with prestressed CFRP strips with gradient anchorage". *Journal of Composites for Construction 17(5): 651-661.*

19. Michels, J.; Barros, J.; Costa, I.; Sena-Cruz, J.; Czaderski, C.; Giacomin, C.; Kotynia, R.; Lees, J.; Pellegrino, and C.; Zile, E. (2016). "Prestressed FRP Systems-Design Procedures for the Use of Composites in Strengthening of Reinforced Concrete." *RILEM State-of-the-Art Reports 19, C. Pellegrino and J. Sena-Cruz (eds.): 263-301.*

20. Nguyen, D.M., Chan, T.K., and Cheong, H.K. (2001). "Brittle failure and bond development length of CFRP concrete beams." *Journal of Composites for Construction*, ASCE 5(1): 12-17.

21. NP EN 1992-1-1. (2010). "Design of concrete structures. Part 1-1: general rules and rules for buildings". *Caparica: IPQ - Instituto Portugues da Qualidade.*

22. NP EN 12390-3. (2011). "Testing hardened concrete. Part 3: compressive strength of test specimens." *Caparica: IPQ - Instituto Portugues da Qualidade.*

23. NP EN ISO 6892-1. (2012). "Metallic materials. Tensile testing. Part 1: method of test at room temperature". *Caparica: IPQ - Instituto Portugues da Qualidade*.

24. Pantuso, A., Neubauer, U. and Rostasy, F.S. (2000). "Effects of thermal mismatch between FRP and concrete on bond." *Proceedings of the 4th ConFibreCrete Meeting, Lille, France.*

25. Sato, Y., Kimura, K., and Kobatake, Y. (1997). "Bond Behaviors between CFRP Sheet and Concrete." *Journal of Structural Construction Engineering, (500): 75-82.*

26. Schmidt J., Bennitz A., Täljsten B., Goltermann P., and Pedersen H. (2012). "Mechanical anchorage of FRP tendons – A literature review". *Construction and Building Materials (32): 110-121.*

27. Sena-Cruz J. (2004). "Strengthening of concrete structures with near-surface mounted CFRP laminate strips". *PhD Thesis, University of Minho, Portugal*.

28. Sena-Cruz, J. (2015) "Project PTDC/ECM-EST/2424/2012 - FRPreDur – Short and long-term structural behaviour of concrete elements flexurally strengthened with prestressed CFRP laminates. Final Report – Scientific Component (Detailed description of the developed task)." *University of Minho, Department of Civil Engineering.*

29. Sena-Cruz J.,Michels J., Harmanci Y., and Correia L. (2015). "Flexural strengthening of RC slabs with prestressed CFRP strips using different anchorage systems". *Polymers (7): 2100-2118.*

30. S&P. (2013). Resin 220 epoxy adhesive, technical datasheet. Seewen, Switzerland. p. 3.

31. S&P. (2014). CFRP laminates, technical datasheet. Seewen, Switzerland. p. 6.

32. Stevens N., Uzumeri S., and Collins M. (1987). "Analytical modelling of reinforced concrete subjected to monotonic and reversed loadings". *Publication No. 87.1. University of Toronto, Toronto.*